The Influence of Network Design Parameters on the Morphology Evolution in Diels-Alder Blends via Thermodynamics and Kinetics Control

Fatemeh Sahraeeazartamar [a], Nirmayi Sadanand Joshi [a], Roos Peeters [c], Bram Vanderborght [b], Guy Van Assche [a], Joost Brancart [a]*

joost.brancart@vub.be

a Lab of Physical Chemistry and Polymer Science (FYSC), Sustainable Materials Engineering Research Group (SUME), Vrije Universiteit Brussel, Pleinlaan 2, B-1050 Brussels, Belgium

b Brubotics, Department of Mechanical Engineering, Vrije Universiteit Brussel and IMEC, Pleinlaan 2, B-1050 Brussels, Belgium

c Materials and Packaging Research & Services (MPR&S), Institute for Materials Research (IMO-IMOMEC), Hasselt University, Wetenschapspark 27, 3590 Diepenbeek, Belgium

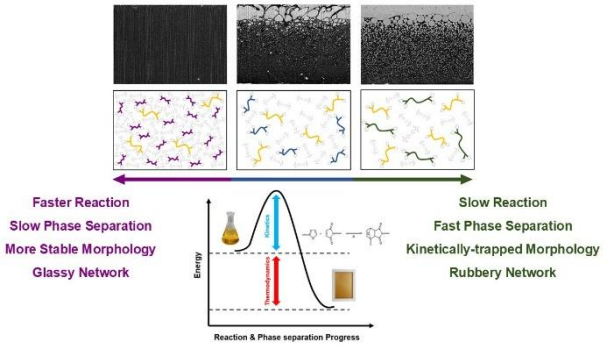

ABSTRACT

Reversible polymer network blends leverage the advantageous properties of the immiscible polymer backbones. Previous work showed that the phase morphology of blends of a hydrophilic poly(propylene oxide) (PPO) and hydrophobic polydimethylsiloxane (PDMS) cured by the reversible Diels-Alder reaction depends on the mass ratio of the two polymers and the maleimide-to-furan ratio used for the reversible network polymerization. This work studies the competition between the reversible Diels-Alder reaction and the phase separation kinetics and thermodynamics to control the phase formation. A furan-functionalized PPO with a molar mass of 4546 g mol^{-1} was blended with furan-functionalized PDMS with different molar mass, mass ratio of the polymers, and stoichiometric ratio. At the highest molar mass of 4961 g mol^{-1}, the PDMS and PPO separate quickly into separate

layers, creating a barrier against both water and oxygen, respectively. The thickness, morphology, and composition of the layer depend on the composition of the blend. At a lower molar mass of the PDMS, the chemistry of the furan end groups becomes more pronounced, which increases the compatibility of the two polymers, reducing the thermodynamic driving force for phase separation. In addition, the increased concentration of furan and maleimide groups increases the Diels-Alder reaction rates and leads to more crosslinked network blends. Mastering the interplay between the thermodynamics of the blends, and the kinetics of the network formation and phase separation by judicious combinations of the network design parameters leads to final blend morphologies ranging from kinetically trapped uniform microstructures to almost completely phase-segregated morphologies. Finally, the solvent extraction time was used as a process parameter of the wet blending process. Slow evaporation of the solvent over the course of one week resulted in a near-equilibrium separation of the two immiscible polymers into separate layers with perfect interfacial bonding by the same Diels-Alder chemistry. Manipulation of these factors enables the development of Diels-Alder network blends with a wide range of properties that are suitable for a wide variety of applications. The fastest and most efficient autonomous healing is achieved at higher PPO contents and for the highest PDMS molar masses, while the best barriers against water and oxygen are obtained at the highest crosslink densities.

KEYWORDS: Polymer Blends, Phase Separation, Dynamic Covalent Networks, Diels-Alder, Self-healing, Permeability.

1. Introduction

Polymer blends combine the best properties of different polymers, offering improved performance, processability, and cost-effectiveness. By blending polymers with complementary characteristics, materials with enhanced strength, toughness, heat resistance, chemical durability, and barrier properties can be created. Blends enable balancing a set of properties that individual polymers may not provide on their own[1]. Polymer blends can be tailored to meet specific needs by adjusting certain properties. This versatility allows the design of materials for a wide range of applications[2]. By adjusting the blend ratio and composition, it is possible to tailor different characteristics to meet specific application requirements. Several methods are used to create polymer blends, including melt mixing, solution mixing, and in situ polymerization[1]. Each method has its advantages and is chosen based on the properties of the polymers as well as the desired properties and processing requirements of the final blend[3].

The phase behavior is the key point in a polymer blend consisting of polymers with varying compatibilities. Polymer blends can exhibit miscibility, phase separation, or various intermediate

levels of mixing, such as partial miscibility[4]. For low molar mass materials, the large combinatorial entropy contribution significantly promotes miscibility. This effect explains why solvent-solvent mixtures a much broader range of miscibility have compared to polymer-solvent combinations. The range of miscible combinations becomes even more limited when dealing with polymer-polymer mixtures. Immiscible polymer blends, where the component polymers do not mix at the molecular level, can exhibit a variety of morphologies after the phase separation process[4]. The phase behavior and final morphology in blends are linked to the thermodynamic and kinetic of the phase separation process.

Kinetically trapped morphology in immiscible polymer blends occurs when different polymer phases are unable to reach their most stable configuration due to rapid processing or insufficient time, resulting in a non-equilibrium state[5]. Ideally, given enough time, these polymers would separate into stable domains. However, quick solidification, high shear rates, or fast reactions during processing can trap the morphology based on processing conditions rather than thermodynamic stability. This can lead to irregular domain sizes, reduced stability, and altered physical properties such as mechanical strength or optical clarity. When phase separation of immiscible polymers coincides with a polymerization or cross-linking reaction, the resulting morphology depends on the competition between the kinetics of the reaction (polymerization rate) and the kinetics of phase separation (rate of domain formation). If polymerization occurs faster, a fine, heterogeneous structure is formed; if phase separation is quicker, larger, more defined domains result[6]. In many cases, kinetics are balanced, leading to complex, interconnected morphologies. Factors like temperature, monomer concentration, and solvents influence this competition, affecting the final material properties.

There has been quite a lot of research on different polymer blends. In recent decades, specific polymer blends can be designed to support sustainability to reduce the overall environmental impact by incorporating polymers that can be recycled and reprocessed[7,8]. This approach helps make polymer materials more eco-friendly and aligns with recycling and waste reduction efforts. As a bridge between thermoplastic and thermosets, dynamic covalent chemistries offer opportunities for the development of a network with both the processability of thermoplastics and the chemical and dimensional stability of thermosets[9]. The reversibility and dynamic of these networks are not only associated with recycling and reprocessing ability, but they also allow recovery of the network in case of any damage referred to self-healing properties[10]. Despite the interesting features that dynamic covalent bonds can provide, their implementation in polymer blends is still limited[11,12].

Several chemistries have been explored in the literature among which Diels-Alder chemistry is one of the most well-known dynamic covalent chemistries[13]. This chemistry is based on a reaction as a type of cycloaddition reaction where a diene (a molecule with two conjugated double bonds) reacts with a dienophile (a molecule that is typically a compound with a double or triple bond, often electron-deficient) to form a six-membered ring called cyclohexene. This reaction is an equilibrium reaction, meaning that the bonds are formed and broken simultaneously in a single step. Once the material is heated the equilibrium is shifted to dissociation of Diels-Alder bonds and vice versa. These bonds function as reversible crosslinks enabling the thermoreversible behavior in the network[14].

The chemistry and the architecture of the Diels-Alder polymer networks formed by these thermoreversible crosslinks can be easily tuned by network design parameters allowing the synthesis of networks suitable for a wide range of processing and application[15]. These parameters include all characteristics of the polymer chain and crosslinkers such as chemistry, molar mass, number of functional groups, and the ratio between two functional groups[16]. When it comes to blending based on the Diels-Alder network, both network design parameters and blend design parameters such as composition are important.

As previously stated, blends are designed for improved performance. Each morphology offers specific improvements in properties. For instance, droplet-matrix morphologies are common in the enhancement of toughness while co-continuous morphologies are known for improved barrier properties[17]. The focus of this work is on polymer blends and the control of their phase behavior for the development of polymer blends used as encapsulants for the preservation of liquid metal used in the fabrication of stretchable sensors[18]. The encapsulants should meet certain requirements such as mechanical stretchability, improved barrier properties against water and oxygen, and good self-healing performance. It was previously studied that blending can be used as a tool to balance contradicting properties where one needs low chain mobility (barrier properties) and the other needs high chain mobility (mechanical stretchability and self-healing properties)[19]. Knowing all the parameters by which the morphology of the blends can be tuned is valuable knowledge for achieving certain properties. The objective of this work is to control the phase behavior of the blended networks by understanding the interplay between the phase separation of two polymers and the Diels-Alder reaction that both happen simultaneously. A thorough comprehension of this process, which is mainly governed by network and blend design parameters, allows the development of blends with a wide range of properties suitable for certain applications.

2. Experimental methods

2.1. Materials

Furfuryl glycidyl ether (FGE) with a molar mass of 154.16 g mol^{-1} and purity of 97% was purchased from BLD Pharmatech GmbH, Kaiserslautern, Germany. A polypropylene oxide-based polyether amine Jeffamine D4000, with an average molar mass of 4546 g mol^{-1} with 2 primary amine end-groups was kindly provided by Huntsman. Aminopropyl-terminated polydimethylsiloxanes DMS A21, DMS A15, and DMS A12, with average molar masses of 4961 g mol^{-1}, 3395 g mol^{-1}, and 907 g mol^{-1}, respectively, all having two primary amine end-groups, were purchased from Gelest. 1,1′-(methylenedi-4,1-phenylene) bismaleimide (DPBM, 95%) and hydroquinone (1,4-benzenediol, 99%) were obtained from Sigma Aldrich. Chloroform (99.9%) was purchased from Biosolve Chimie. All chemicals were used as received. Some of the structures are shown in Scheme 1.

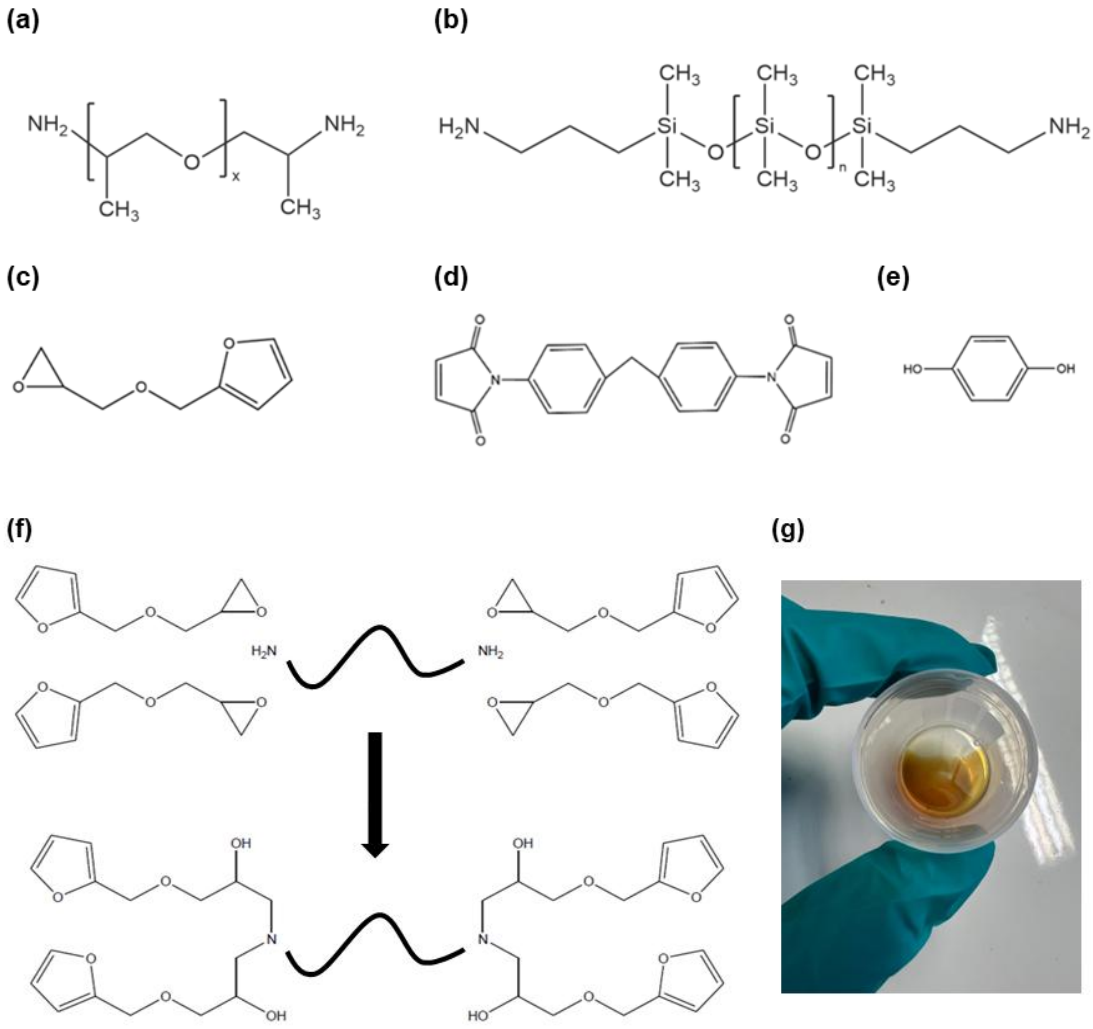

Scheme 1. Chemical structure of all monomers used in the synthesis of the Diels–Alder polymer networks: (a) polyether amine JD4000 with x=49.0, (b) aminopropyl dimethyl siloxane chains DMS950, DMS3000, and DMS5000 with different numbers of repeating units (different molar mass) n = 8.9, 42.5, and 63.7, respectively,

(c) furfuryl glycidyl ether (FGE), (d) 1,1′- (methylenedi-4,1-phenylene) bismaleimide (DPBM), and (e) 1,4-benzenediol (hydroquinone). (f) Irreversible epoxy-amine reaction used for furan functionalization of prepolymers. (g) The physical appearance of two immiscible polymers after functionalization and before crosslinking**.**

2.2. Synthesis of Diels-Alder network blends

The synthesis of DA network blends was performed in two steps. First, Jeffamine D4000 and aminopropyl-terminated polydimethylsiloxanes DMS A21, DMS A15, or DMS A12, were separately functionalized with furan groups via an irreversible epoxy-amine reaction with furfuryl glycidyl ether (FGE), as shown in Scheme 1. This reaction was carried out under stoichiometric conditions between amine hydrogens and epoxide groups ([amine NH]/[epoxy] = 1). The mixtures were placed in an oil bath at 60 °C and magnetically stirred for 5 days, after which the temperature was raised to 90 °C for 2 days to complete the epoxy-amine reaction. After the completion of this reaction, the molar mass and functionality of furan-functionalized PDMS chains were confirmed by ^{1}H NMR spectroscopy (see Supporting Information).

The furan-functionalized Jeffamine FD4000 was mixed with one of the furan-functionalized polydimethylsiloxanes (FS5000, FS3000, or FS950), dissolved in chloroform, and crosslinked with bismaleimide DPBM in a selected maleimide-to-furan stoichiometric ratio so called $r = [M]/[F]$. To avoid the side reactions due to the presence of maleimide, especially the radical-induced homopolymerization of maleimide, hydroquinone was added to the mixture as a radical inhibitor. The mixtures were stirred by a magnet stirrer for at least 6 hours to ensure the dissolution of the solid DPBM and to achieve excellent mixing of all components in the solution. Two types of polymer networks, one based on PPO segments named DPBM-FD4000_r0.7 and the other based on PDMS segments named DPBM-FS5000_r0.7, DPBM-FS3000_r0.7, and DPBM-FS950_r0.7 (depending on the molar mass), were obtained. These pure networks were synthesized by a solvent casting procedure followed by extracting the chloroform for 24 hours at room temperature in a vacuum oven equipped with a liquid nitrogen cold trap. In this step, the evaporation of the solvent leads to the increased concentration of maleimide and furan reacting groups, pushing the reaction equilibrium toward the formation of DA cycloadducts as reversible covalent bonds.

Blends of network DPBM-FD4000_r0.7 with one of the networks DPBM-FS5000_r0.7, DPBM-FS3000_r0.7, or DPBM-FS950_r0.7 were produced by mixing the furan-functionalized precursors in different mass ratios, followed by crosslinking the precursor mixture using DPBM, using the same protocol as for the pure networks. Table 1 shows the compositions of the blends. Moreover, 50/50

blends were made at the lower maleimide-to-furan stoichiometric ratios of 0.6 and 0.5 to investigate the effect of crosslink density and reaction kinetics on the formed blends.

Table 1. List of the prepared pure and blended PPO-based and PDMS-based Diels-Alder networks. In this nomenclature, X represents the molar mass of PDMS backbones.

Network (Pure/Blend)	Network 1 (PPO)	Network 2 (PDMS)	Mass Ratio (Composition)	Stoichiometric Ratio
DPBM-FD4000_r0.7	DPBM-FD4000_r0.7	-	100/0	0.7
blend 7525_r0.7_X	DPBM-FD4000_r0.7	DPBM-FSX_r0.7	75/25	0.7
blend 5050_r0.7_X	DPBM-FD4000_r0.7	DPBM-FSX_r0.7	50/50	0.7
blend 2575_r0.7_X	DPBM-FD4000_r0.7	DPBM-FSX_r0.7	25/75	0.7
blend 5050_r0.6_X	DPBM-FD4000_r0.6	DPBM-FSX_r0.6	50/50	0.6
blend 5050_r0.5_X	DPBM-FD4000_r0.5	DPBM-FSX_r0.5	50/50	0.5
DPBM-FSX_r0.7	-	DPBM-FSX_r0.7	0/100	0.7

2.3. Characterization techniques

2.3.1. Scanning electron microscopy (SEM)

The microstructure and morphology of the bulk of the polymer blends possessing different compositions and stoichiometric ratios and made with different PDMS grades varying in molar mass were investigated by scanning electron microscopy (SEM) using a JEOL JSM-IT300 system. The backscattered electron images showing the composition of the blends (BED-C) were taken using an acceleration voltage of 20 kV and a probe current of 60 A at a working distance of 9−10 mm. The coupled energy-dispersive X-ray spectroscope (EDX) was utilized to collect the elemental maps of carbon and silicon atoms from the cross-sectional area of the blends. The electron images were obtained with 100 times magnification using beam energy with an accelerating voltage of 20 kV.

2.3.2. Thermogravimetric analysis (TGA)

The thermal stability of the network blends was studied using thermogravimetric analysis (TGA) on a TA Instruments TGA Q5000IR. Samples with a mass of around 0.5 mg were heated up to 600 °C at a heating rate of 10 K min^{-1}. All measurements were performed under a nitrogen flow rate of 25 mL min^{-1} since an inert environment was required.

2.3.3. Differential scanning calorimetry (DSC)

The thermophysical properties of the polymer networks were studied by conventional differential scanning calorimetry (DSC) using a TA Instruments Q2000 DSC equipped with a liquid nitrogen cooling system (LNCS) and using helium as the purge gas. For all the pure and blended networks, heat-cool-heat cycles were performed between -150 and 150 °C at the same heating/cooling rate of 10 K min^{-1}. Samples having a mass of 10-15 mg were placed in Aluminium T_{zero} pans and sealed with a hermetic lid supplied by TA Instruments. The data of the second heating were used to avoid the influence of the thermal history of samples.

2.3.4. Dynamic mechanical analysis (DMA)

To evaluate the viscoelastic properties of different pure and blended networks, a TA Instruments DMA Q800, equipped with a gas cooling accessory (GCA) was utilized. At a frequency of 1 Hz and applying a strain amplitude of 0.1%, small amplitude oscillatory tensile measurements were performed on rectangular specimens having dimensions of 15 mm × 3 mm × 1 mm. Using these measurements, the storage modulus, loss modulus, and tangent of the loss angle ($tan\ \delta$) of polymer networks were derived as a function of temperature. After equilibrating at -130 °C, all samples were subjected to a heating temperature ramp between -130 and 110 °C at the rate of 5 K min^{-1}, using a force track of 125%. The glass transition temperatures were determined as the peak maxima of the loss modulus.

2.3.5. Dynamic rheometry

Dynamic rheometry was performed with a TA Instruments Discovery Hybrid Rheometer (DHR2) to study the viscoelastic properties of pure and blended networks as well as their gel transition temperature. The experiments were performed using a 15 mm Aluminium parallel plate geometry. Samples in the shape of a disk with 15 mm diameter and 1 mm thickness were subjected to an oscillatory strain with an amplitude of 5% at frequencies of 0.312, 0.562, 1.00, 1.778, and 3.125 Hz. After 5 minutes of soaking at 40 °C, the samples underwent a heating ramp of 1 K min^{-1} in a temperature range between 40 and 120 °C.

2.3.6. Dynamic vapor sorption analysis (DVS)

Dynamic vapor sorption analysis (DVS) was conducted to quantify the solubility of water in the polymer through pure and blended networks. This gravimetric sorption analysis method was performed using a TA Instruments Q5000 sorption analyzer (Q5000 SA), employing nitrogen as the purge gas. The weight change of polymer samples due to sorption or desorption was measured at a controlled temperature of 25 °C in a controlled water vapor atmosphere having relative humidity values of 0%, 50%, and 98% to mimic a dry state, standard indoor application conditions, and maximum humidity

conditions, respectively. To optimize the test conditions and to obtain reliable results, polymer specimens with an average thickness of 150 µm and a surface area of 6 mm × 6 mm were exposed to each relative humidity in an isothermal step with a duration of 360 minutes. After these isothermal steps, the samples were dried to 0% relative humidity at a rate of 0.5% min^{-1}.

2.3.7. Water vapor transmission rate (WVTR)

To measure the rate at which water vapor permeates through the pure and blended networks, water vapor transmission rate measurements (WVTR) were performed utilizing a MOCON Permatran-W Model MG WVTR module, adhering to ASTM F-1249, the standard test method for WVTR through plastic films and sheeting. These measurements were performed at the MPR&S lab in the Institute for Material Research of Hasselt University (Belgium). The test conditions included maintaining a temperature of 25°C while the relative humidity conditions were set to 50% RH on one side of the polymer sample and 0% RH on the other, with a free orientation of the test sample. The polymer samples with thicknesses ranging from 100 µm to 400 µm were fixed in between 2 aluminum stickers with a circular opening that has an area of 5 cm^2. To avoid microchannels, epoxy glue was applied at the border of the test sample and the mask (on both sides of each sample). WVTR values were measured in g $m^{-2}.day^{-1}$.

2.3.8. Oxygen transmission rate analysis (OTR)

The permeation of oxygen through pure and blended networks was evaluated by oxygen transmission rate (OTR) studies using a MOCON OX-TRAN model 2/21 instrument in a dual film test cell module according to the ASTM-F-1927. These measurements were performed at the MPR&S lab in the Institute for Material Research of Hasselt University (Belgium). The oxygen transmission rate (in cc/m2. day) of solvent-casted polymer sheets with thicknesses ranging from 100 µm to 400 µm was measured at 25 °C through a comparative test using a relative humidity of 50 %. In practice, 5% oxygen was exploited as testing gas. Finally, the OTR values were recalculated for 100% oxygen. Additionally, nitrogen was used as a carrier or purge gas to create an oxygen-free environment on one side of the test material.

2.3.9. Mechanical and self-healing tests

Tensile testing measurements were carried out at room temperature using a TA Instruments DMA Q800, equipped with a gas cooling accessory (GCA). Stress-strain curves were obtained in controlled strain rate mode using a tension clamp (TA Instruments) suitable for film specimens. Rectangular specimens with dimensions of 15 mm × 3 mm × 1 mm were cut from the solvent-casted sheets and clamped with a length of 5 mm. Specimens were subjected to a strain rate of 60% min^{-1} using a preload

force of 0.01 N, and an initial strain of 0.2%. The mechanical properties were determined from the average values of at least five replicates for each network. Young's modulus was determined in the initial linear region of the stress-strain curve (0-0.5% strain).

In addition, to elucidate the mechanical hysteresis of pure and blended networks at room temperature, five loading-unloading cycles were performed at a stress ramp of 0.1 MPa min^{-1} in which the samples were strained to a maximum stress of 0.2 MPa.

To study the mechanical healing efficiency of the polymer networks rectangular sheets of DA network samples were cut in two parts, which were immediately brought back into contact, and kept at either room temperature (25 ºC) or 60 ºC for 1 week. After the healing step, the healed rectangular sheet was cut perpendicularly to the scar and split into five healed strips with dimensions of 15 mm × 3 mm × 1 mm. All samples were tested in a controlled strain mode at room temperature following the same test conditions as mentioned earlier for tensile testing.

3. Results and discussion

3.1. Design parameters in Diels-Alder network blends

The architecture of DA networks determines their properties and potential applications. This network architecture is influenced by several parameters, so by changing these parameters the characteristics of DA networks can be easily tailored[20,21]. For a fixed diene and dienophile, in this case, a furan and a maleimide, other parameters such as chemistry, molar mass, functionality, and the stoichiometric ratio between maleimide and furan functional groups (Scheme 2a) significantly influence, not only the polymer network properties[22,23,24], but also on the kinetics of the network formation and its thermo-reversibility[19]. The chemistry of the prepolymer not only affects the hydrophobicity, flexibility, stability, density, and viscosity of the polymer chain but also impacts other thermo-physical properties of the network, such as the glass transition temperature, the crystallization ability, and the resulting melting temperature. The molar mass affects all physical, thermal, and mechanical properties. Moreover, in a network structure, the lower the molar mass of the prepolymer, the lower the average distance between crosslinks, and the higher the crosslink density. In addition, the functionality of the prepolymer plays an important role. Increasing the number of functional groups in a constant molar mass leads to a higher crosslink density, affecting the properties of a network. A polymer network with a higher crosslink density is less flexible because the chain mobility is constrained by the high number of effectively elastic junctions. Finally, in dynamic covalent networks, such as DA networks, the maleimide-to-furan stoichiometric ratio has a big influence on the network characteristics. Bringing this ratio closer to one increases the number of DA bonds resulting in a network with a higher fraction of elastically active chains, or a lower fraction of dangling or unconnected chains. Regardless of the

choice of the reagents, the synthesis and processing conditions, such as temperature, catalyst, solvent, and time have additional impacts.

The blending approach of two polymers crosslinked with dynamic covalent bonds, particularly DA bonds, for tuning mechanical and self-healing properties has been investigated before[25,26]. Our previous study showed that blending two immiscible polymers with different chemistries and crosslinking them with DA reaction renders new possibilities/challenges in the design of networks with enhanced barrier properties[27]. To embark on a new investigation and understand more about these phase-separated blends, the molar mass of the second polymer meaning PDMS was changed while other parameters remained unchanged. So, in a 50/50 mass ratio, PPO-based polymer FD4000 was combined with siloxane-based polymer chains DMS5000, DMS3000, or DMS950, which differ in molar mass, while all possessing four furan moieties. The mixture was subsequently crosslinked with a DPBM, containing two maleimide moieties in a stoichiometric ratio of r=0.7. The molar mass of PDMS chains, the only variable in these network blends, has a significant effect on the concentration of the reacting groups and the network properties. By choosing a constant composition of 50/50 and a stoichiometric ratio of r=0.7, as demonstrated in Scheme 2b in blends containing PDMS chains with a lower molar mass, the concentration of functional furan and maleimide groups capable of forming DA bonds (reversible crosslinks) is higher compared to blends containing higher molar mass PDMS chains. This increased concentration of reacting groups means more opportunities for crosslink formation per unit volume, typically resulting in a higher crosslink density and *vice versa*. Altering the length of the PDMS not only affects the kinetics due to the change in concentration of reacting groups but also affects the compatibility of the two immiscible (at high molar mass) polymers by acting on the thermodynamics of the network blends. Changing the driving forces for the kinetics and thermodynamics of DA networks results in various phase behaviors and different morphologies of the network blend since the morphology evolution revolves around these two key points.

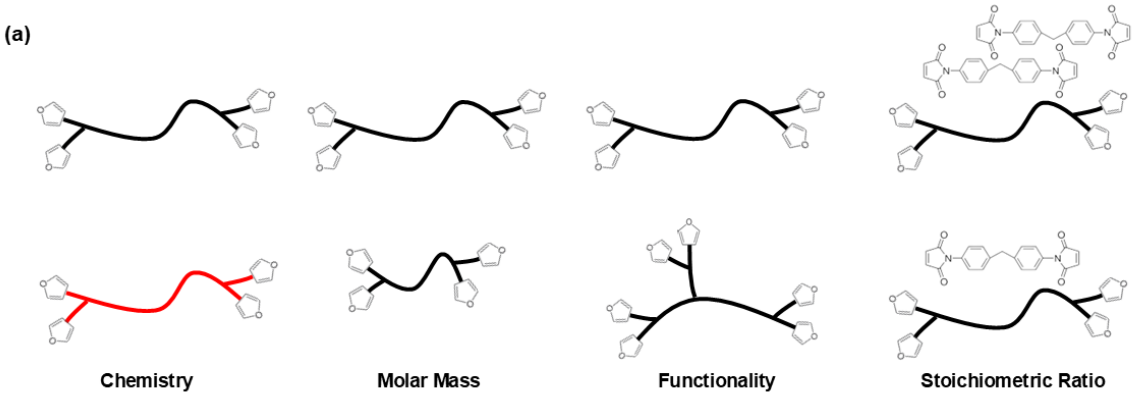

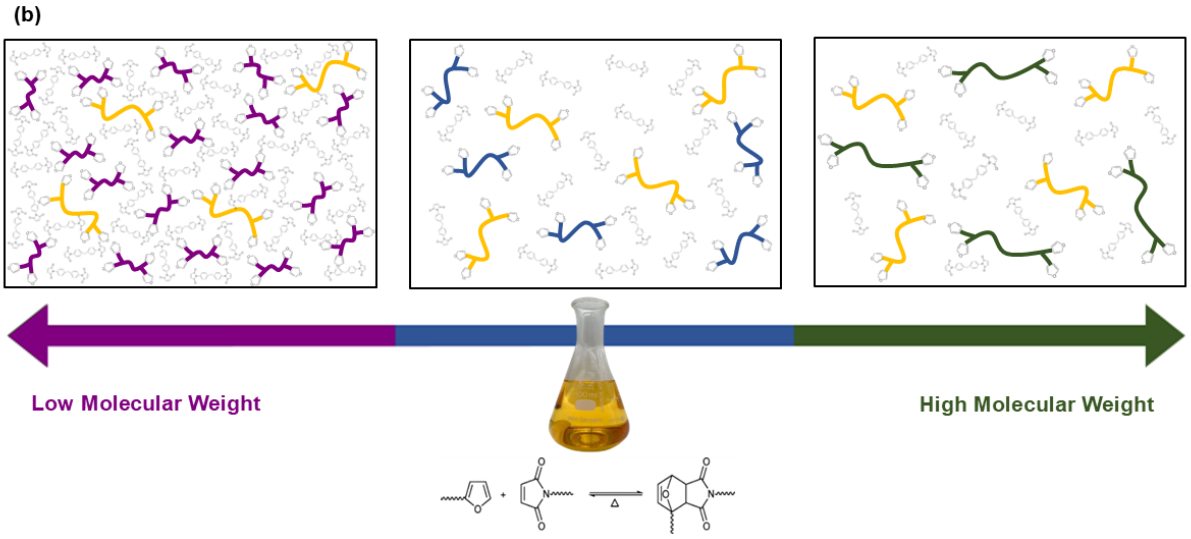

Scheme 2. (a) Demonstration of different network design parameters in a furan-functionalized polymer chain. (b) Influence of the molar mass of polydimethylsiloxane chains on the concentration of furan and maleimide reacting groups in a mixture of both polymers at a constant composition and maleimide-to-furan stoichiometric ratio.

3.2. Morphology of Diels-Alder network blends

The morphology of the DA polymer blends was studied using scanning electron microscopy (SEM). The cross-section of the DA network blends having different PPO/PDMS mass ratios is shown by their backscattered electron SEM images (Figures 1a-i). These micrographs depict the effect of the composition of the blend in three different series of blends: the combination of FD4000 with long chains of FS5000 (Figures 1a-c), the combination of FD4000 with medium chains of FS3000 (Figures 1d-f), and finally the combination of FD4000 with short chains of FS950 (Figures 1g-i). As discussed in the previous work[27], at low concentrations of FS5000, the FD4000/FS5000 mixture forms a droplet-dispersed morphology. This morphology evolves with the formation of a thick layer of PDMS at higher concentrations of FS5000. At constant composition and stoichiometric ratio, in blends made with shorter PDMS chains such as FS3000 and FS950, the phase behavior changes towards more homogeneous morphologies. It is understood that in the case of FS950, the blends are thermodynamically more stable. The first reason comes from the faster DA reaction in the blends made with shorter PDMS chains. At a constant stoichiometric ratio $r = 0.7$, decreasing the polymer length leads to a higher concentration of the reacting groups at the start of the reaction $[i]_0$, which increases the speed of the DA reaction and results in faster gelation, and at equilibrium $[i]_{eq}$. The second reason is related to the slower phase separation of the blends made with shorter PDMS chains. The shorter PDMS chains are more compatible with FD4000, owing to their higher furan content, a functional group they have in common (Scheme 3). Moreover, the effect of low molar mass in the increase of the

combinatorial contribution of the mixing entropy should not be neglected[28]. This improved compatibility retards the phase separation process: as shown in Scheme 3c, FS950 could not segregate from FD4000 even after one month. Therefore, the final morphology is kinetically trapped[29,30], the morphology being a product of competition between relatively fast reaction kinetics and slow phase separation kinetics. On the other hand, blends made with longer PDMS chains meaning FS5000 behave the opposite. In these blends, as shown also in our pervious study, the longer chains are associated with fewer end groups meaning fewer reacting groups. Fewer reacting groups not only yield slower reaction rates but also decrease the compatibility of two furan functionalized chains and accelerate the phase separation process. A slower reaction rate combined with a faster phase separation process tends to produce blends with a higher degree of heterogeneity.

Table 2. Functional molar masses and concentrations of maleimide and furan reacting groups at the start of the reaction and concentrations of reactants and Diels-Alder adducts in equilibrium condition (25 °C) calculated by kinetic simulation using the kinetic parameters[15].

Material	$[M]_0$ (mol kg^{-1})	$[F]_0$ (mol kg^{-1})	$[M]_{eq}$ (mol kg^{-1})	$[F]_{eq}$ (mol kg^{-1})	$[A]_{eq}$ (mol kg^{-1})
DPBM-F4000_r0.7	0.49	0.71	0.013	0.218	0.487
DPBM-FS5000_r0.7	0.46	0.65	0.014	0.203	0.450
DPBM-FS3000_r0.7	0.68	0.97	0.009	0.298	0.672
DPBM-FS950_r0.7	1.35	1.93	0.005	0.587	1.346

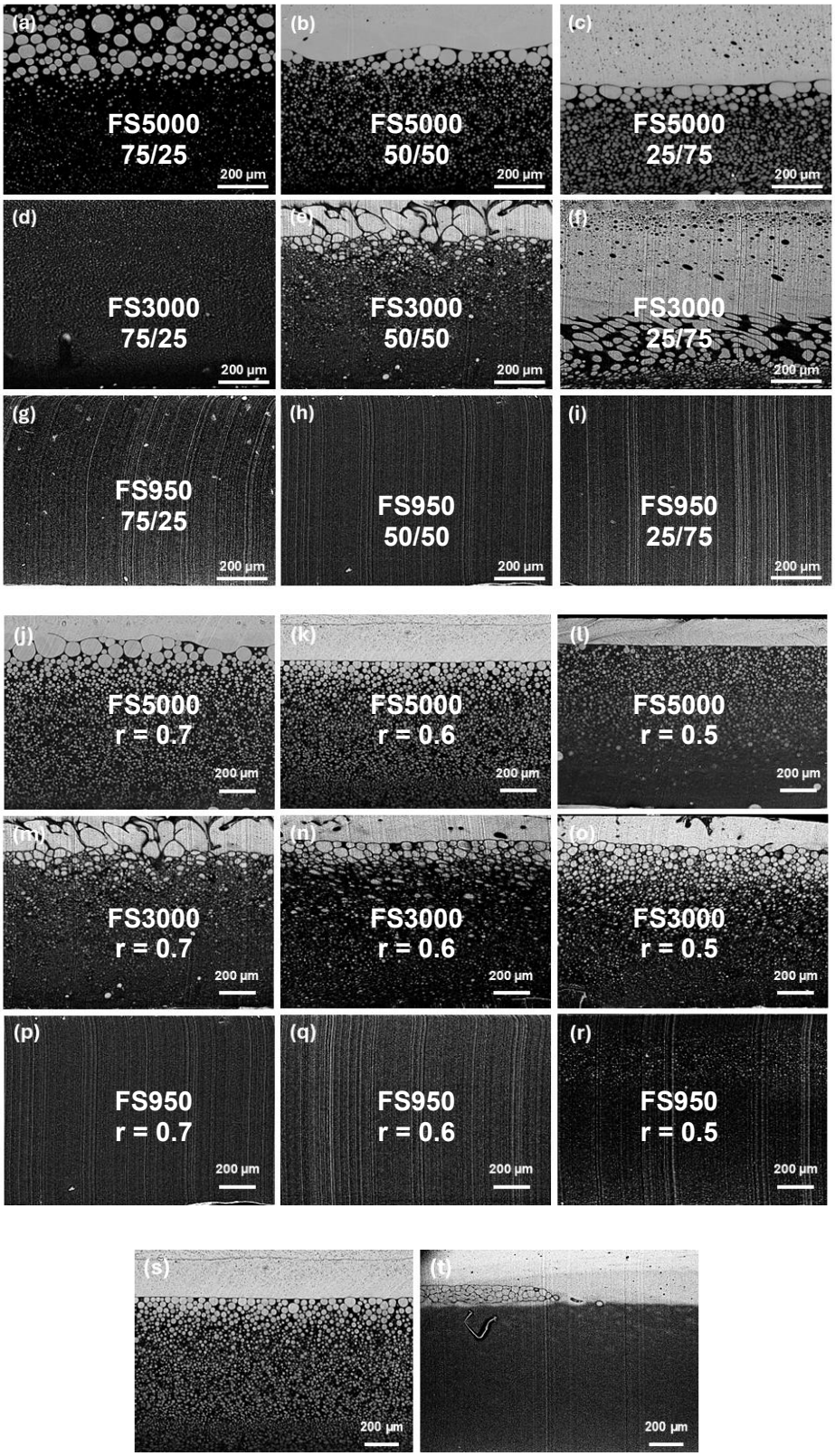

Figure 1. The morphology of the cross-section of the reversible polymer network blends, visualized by scanning electron microscopy of F4000 and FS5000 (a-c), F4000 and FSS3000 (d-f) and F4000 and FS950 (g-i) with a stoichiometric ratio of 0.7 and changing mass ratios of 75/25 (left), 50/50 (middle) and 25/75 (right) shown by first nine micrographs. Second nine micrographs show morphology of blends with a fixed mass ratio of 50/50

for F4000 and FS5000 (j-l), F4000 and FSS3000 (m-o) and for F4000 and FS950 (p-r) and changing stoichiometric ratios of 0.7 (left), 0.6 (middle) and 0.5 (right). Last two micrographs show different morphologies in blend 5050_r0.6_5000 made in two ways: cast in a vacuum oven with 200 m bar pressure with fast evaporation of the solvent and cured in over one day (s) and one week without applying any vacuum so with slow evaporation of the solvent (t).

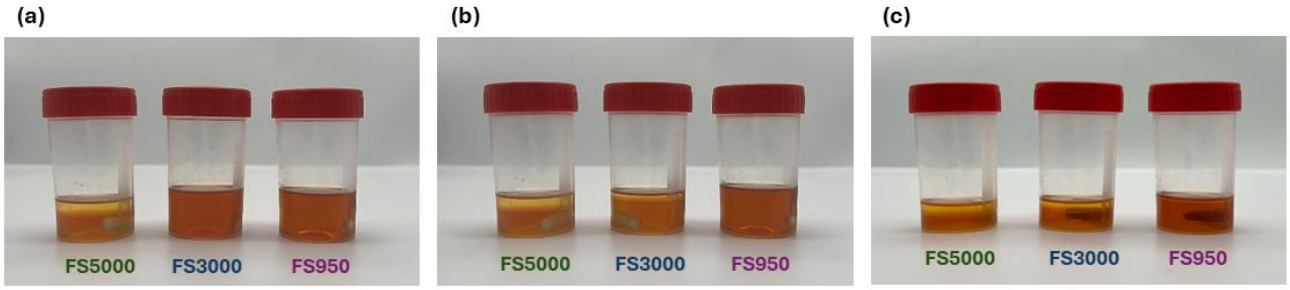

Scheme 3. Phase separation of FD4000 with FS5000 (left), FS3000 (middle), and FS950 (right) with a mass ratio of 50/50 after 1 week (a), 2 weeks (b), and 1 month (c) in chloroform (without the addition of the DPBM crosslinker). The mixtures were prepared and stored at ambient temperature (25 ^{o}C). The mass loss over time is due to the evaporation of chloroform.

To study the effect of the stoichiometric ratio on the phase behavior of the network blends, dynamic network blends were made with different maleimide-to-furan stoichiometric ratios at a constant 50/50 mass ratio of PPO/PDMS (Figures 1j-r). The SEM micrographs show that regardless of the molar mass of the PDMS; by decreasing the stoichiometric ratio all network blends go through phase separation to a higher extent. Even blend 5050_r0.5_950 (Figure 1r) shows a droplet-dispersed phase separation by forming droplets of less than 10 µm. For a constant molar mass of polymers, the decrease in the stoichiometric ratio decreases the concentration of reacting groups and slows down the kinetics of the DA reaction compared to the kinetics of the phase separation, which means there is more opportunity for phase separation to proceed. Finally to study the effect of synthesis conditions and to once more prove the effect of phase-separation and reaction kinetics on the morphology evolution, blend 5050_r0.6_5000 was made in two ways; First, it was cast in a vacuum oven under 200 m bar pressure with fast evaporation of the solvent and cured in over one day shown in Figure 1s and second it was cast in a vacuum oven without applying any vacuum and kept for one week (slow evaporation of the solvent) which is shown in Figure 1t. Reducing the speed of solvent evaporation yields blend with the complete separation of two phases in a fashion that both phases locate in their favored state. Accordingly, their properties will be different.

3.3. Thermo-physical properties of Diels-Alder network blends

Thermogravimetric analysis shows the thermal degradation behavior of different pure and blended DA networks. The rate of thermal degradation and the temperature at which these polymer networks degrade provide valuable insights into their structural characteristics. Figure 2a shows that after a similar slow initial mass loss, the degradation of the PPO-based DA network rapidly accelerates around 350 °C, while the PDMS-based DA networks more gradually degrade. A slower thermal degradation of pure PDMS-based DA networks implies stronger bonds in these polymers. In general, PDMS chains degrade more slowly since their Si-O-Si bonds require more energy to break (on average 452 kJ mol^{-1} for Si-O compared to 347 kJ mol^{-1} for C-O in PPO[31]). By comparing PDMS-based DA networks in Figure 2a it can be concluded that the thermal stability of the three networks depends on their molar mass; the higher molar mass of the polymer chain enhances the thermal stability of the network. In irreversible polymer networks, high crosslink density improves thermal stability since crosslinks create a three-dimensional network that resists thermal motion and degradation[32,33]. However, in reversible DA network DPBM-FS950_r0.7 with the highest density of crosslinks shows the lowest thermal stability. This is related to the lower thermal energy required to volatilize the shorter furan-functionalized prepolymers. Figures 2b-d state that the thermal degradation behavior of the blends is a function of the mass ratios of the PPO and PDMS phases in the blend. The inversion of thermal degradation behavior in blends of FD4000 and FS950 after their crossover (Figure 2d) clearly shows the effect of blending on the degradation behavior of these adaptive covalent networks.

The thermo-physical properties of the network blends were investigated by differential scanning calorimetry (DSC). DSC thermograms for pure and blended DA networks made with three different PDMS chains are given in Figures 2e-g. The glass transition temperature T_g of PDMS and PPO phases are detected at about -120 °C and -60 °C, respectively (Figures 2e and 2f). Regardless of the composition and the stoichiometric ratio of the two polymers in the blends, the glass transition temperatures of the PDMS and PPO phases remain unchanged. This implies their composition is always the same, and thus close to the composition of the pure networks. In general, the height of the glass transition step is proportional to how much of each phase is present in the network blend. This is visible in the case of blends made with FS5000 and FS3000. By changing FS5000 or FS3000 for FS950, the step of glass transition temperature correlated to the PDMS phase shifts to a much higher temperature of about 75 °C. This high glass transition temperature is an indication of a glassy network formed because of short PDMS chains crosslinked with a higher concentration of aromatic bismaleimide units. In blends containing FS5000, above the glass transition of the PDMS phase, exothermic cold crystallization peaks are followed by endothermic melting peaks of PDMS crystals,

which overlap with the steep increase of the glass transition of the PPO phase around -60 °C (Figure 2e). Decreasing the molar mass of the PDMS not only increases the glass transition temperature of the networks but also decreases the probability of crystallization as a result of higher crosslink density and chain confinement effects[34]. Additionally, the size of the PDMS phases might be too small for crystallization. In general, the pure PDMS-based network DPBM-FS5000_r0.7 shows no crystallization in DSC measurements while in DMA measurements (Figure 3) it shows a partial crystallization. The reason is that the heating rate in two methods are different. A fast heating/cooling with a rate of 10 K min^{-1} limits the crystallization of the FS5000, while in DMA a rate of 5 K min^{-1} is slower and promotes the crystallization effect in the longest PDMS chains of FS5000.

The DA reaction between the furan and maleimide reacting groups that remained unreacted during cooling is visible as an exothermic peak at around 50 °C[27]. Increasing the concentration of DA groups by decreasing the PDMS chain length (Table 2) amplifies this exothermic behavior of the blends, as most clearly seen in those containing FS950. Increasing the temperature above 100 °C shifts the DA reaction equilibrium towards the dissociation of the endo and exo stereoisomers in all pure and blended DA networks (double endothermic peaks)[35]. The shape of the endothermic peaks is drastically different after they overlap with the T_g of the PDMS phase at around 90 °C in the blends based on FS950 (Figure 2g). The intensity of the endothermic peaks increases due to the increased molecular motion and changes in thermal properties during the glass transition occurring at these temperatures.

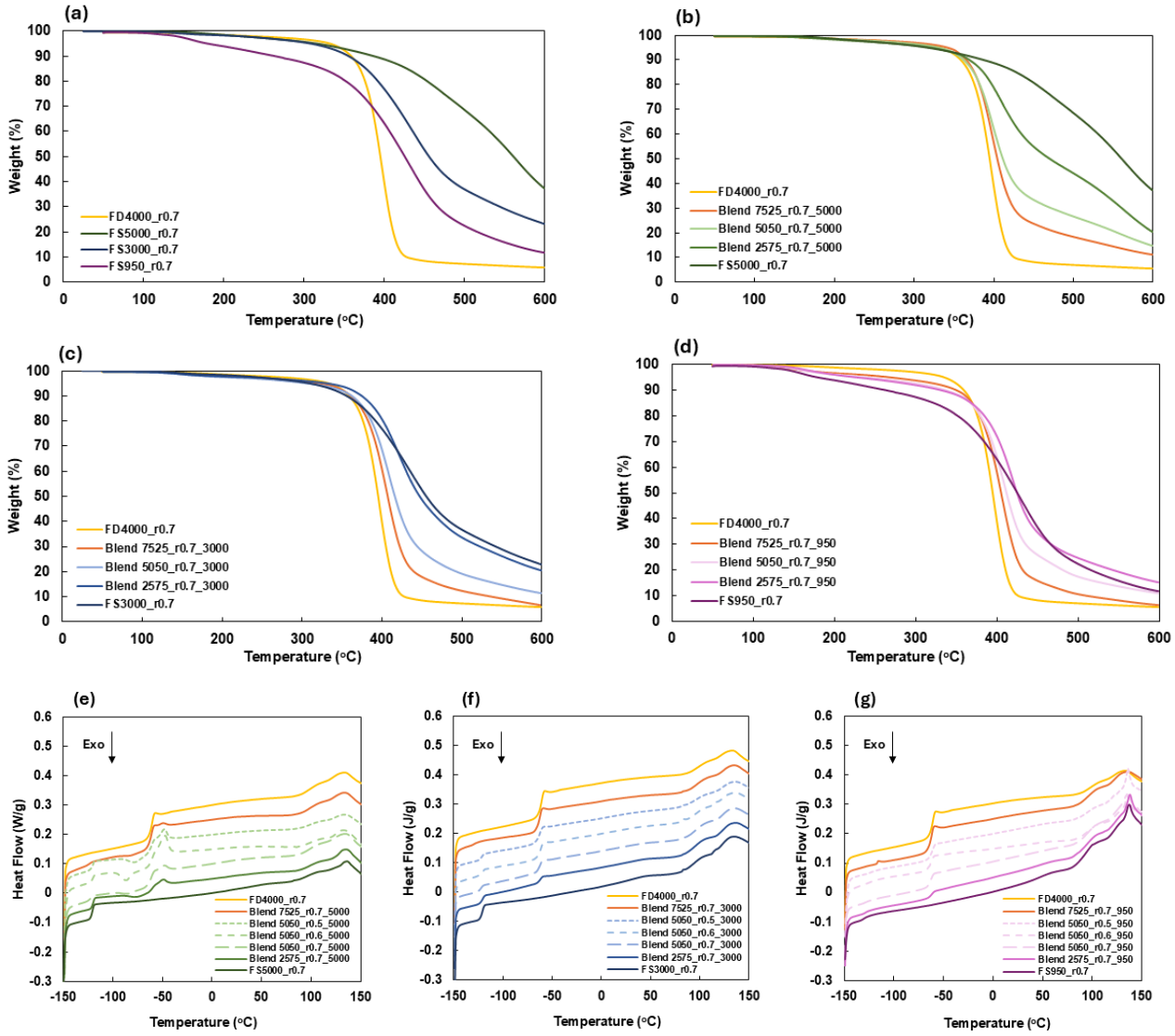

Figure 2. Thermogravimetry thermograms of (a) pure PPO-based FD4000 and PDMS-based Diels-Alder networks with different molar masses of 5000 g mol^{-1} (FS5000), 3000 g mol^{-1} (FS3000), and 950 g mol^{-1} (FS950) crosslinked at r=0.7. Mass loss curves as a function of the temperature in pure and blended Diels-Alder networks with different compositions containing FS5000 (b), FS3000 (c), or FS950 (d) at a stoichiometric ratio of r=0.7. All curves were measured with a heating ramp of 20 K min^{-1}. Differential scanning calorimetry thermograms of pure and blended Diels-Alder networks with different compositions and stoichiometric ratios containing FS5000 (e), FS3000 (f), or FS950 (g) measured at a temperature ramp of 10 K min^{-1}.

3.4. Viscoelastic properties of Diels-Alder network blends

The storage modulus E', loss modulus E'' and loss angle δ were studied over a wide temperature range for the pure networks (Figures 3a-c) and their blends (Figures 3d-i). The DMA measurements confirm the T_g of around -120 °C for the FS5000- and FS3000-based networks, -60 °C for the FD4000-based network and 72 °C for the glassy FS950-based network. The most loosely crosslinked PDMS-based

network DPBM-FS5000_r0.7 shows a broad peak in the storage and loss moduli between -80 and -60 °C, which is attributed to the partial crystallization of PDMS, followed by melting between -60 to -40 °C upon further heating. The lower PDMS chain length and higher crosslink density in the FS3000- and FS950-based networks limits the chain mobility and prevents crystallization. These results are consistent with the observations in DSC (Figures 2e-g). Moreover, the storage modulus of the three networks increases upon reducing the molar mass of the PDMS (Figures 3a-c). DPBM-FS3000_r0.7 shows a clearly increased rubbery plateau modulus compared to DPBM-FS5000_r0.7. DPBM-FS950_r0.7 has the highest modulus due to the high T_g. DPBM-FS950_r0.7 doesn't show a rubbery plateau above its T_g, as at that temperature the DA Adducts already start to gradually dissociate, which can also be observed for the other networks. This is apparent by the decreasing slope of the moduli for all networks.

The PDMS-based network DPBM-FS5000_r0.7 has a lower T_g and a lower plateau modulus than PPO-based network DPBM-FD4000_r0.7 (Figure 3d), due to the higher flexibility of the Si-O chains at similar crosslink density and the same temperature. The 50/50 blend of these two networks shows both glass transitions, as was also observed in DSC (Figure 2e). A first plateau can be observed between the T_g of the PDMS and PPO phases, where the PDMS phase has devitrified, and the PPO phase is still glassy. A second (rubbery) plateau can be observed above the T_g of the PPO phase, where the material has completely devitrified. The same observations can be made for the 50/50 blend of FS3000 and FD4000, with more pronounced intermediate properties compared to the two pure networks (Figure 3e).

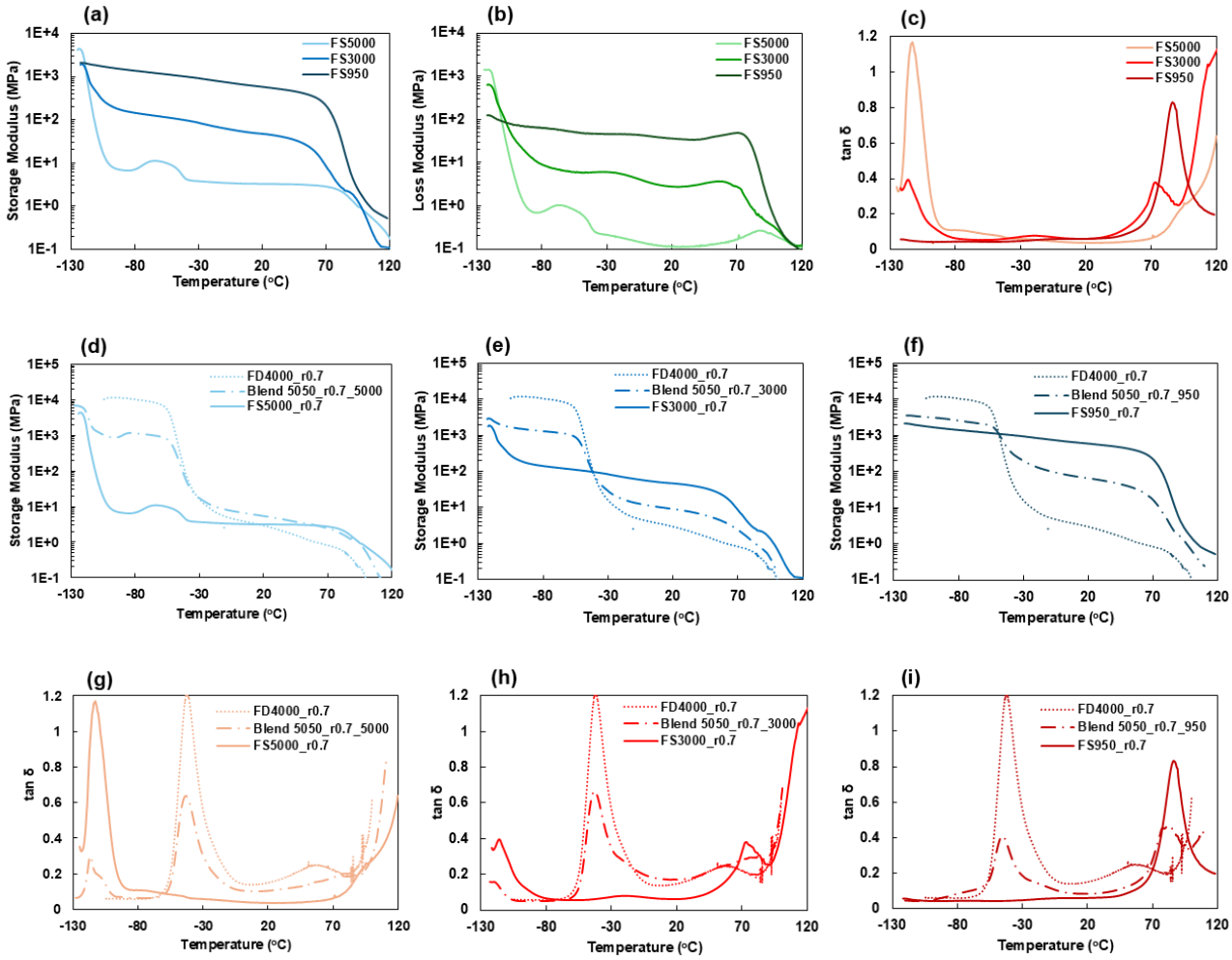

Figure 3. Viscoelastic properties in terms of storage modulus, loss modulus, and tan delta for pure PDMS-based Diels-Alder networks with different molar masses of 5000 g mol^{-1} (FS5000), 3000 g mol^{-1} (FS3000), and 950 g mol^{-1} (FS950) crosslinked at r=0.7 (a-c). Storage modulus (d-f) and tan delta (g-i) of pure Diels-Alder networks and their blend 5050_r0.7 built on FD4000 with FS5000, FS3000, or FS950 measured by dynamic mechanical analysis with a heating speed of 2 K min^{-1}.

Upon further heating the DA networks and their blends, the thermoreversible networks eventually transition from solid to liquid as they pass their gel transition temperature (T_{gel}). The gel transition temperature (T_{gel}) is crucial for (re)processing and applying DA networks. It is observed as the point where the phase angle becomes independent of the oscillation frequency in dynamic mechanical analysis (Figure S2 in Supporting Information). Figure 4 presents the results of dynamic rheometry experiments conducted at a heating rate of 1 K min^{-1} and a frequency of 1 Hz, using an oscillatory strain amplitude of 5%. Figures 4a-c, 4d-f, and 4g-i depict the storage modulus (G'), loss modulus (G''), and phase angle (δ) of pure and blended DA networks with different compositions and stoichiometric ratios containing FS5000, FS3000, and FS950. The storage modulus of PPO-based DPBM-FD4000_r0.7 drops significantly at temperatures above 75 °C, indicating the breakdown of the

polymer network structure due to the dissociation of the DA adducts beyond the critical gel conversion temperature, termed as the gel transition temperature. This observation is supported by the sharp increase of phase angle that approaches 90° signifying the gel transition temperature. PDMS-based DA networks maintain their network structure at higher temperatures (longer rubbery plateau) due to their stronger DA bonds. The explanation would be that since DPBM-FD4000_r0.7 and DPBM-FS5000_r0.7 have a comparable density of crosslinks, while the degelation of PDMS-based network requires much higher energies it can be concluded that DA bonds in PDMS-based network are stronger. Networks predominantly consisting of PPO show a monotonic increase in phase angle (decrease in modulus) above 80 °C due to DA bond dissociation, whereas networks mainly composed of PDMS exhibit a step-like behavior, possibly attributed to endo to exo transformation. Not only do networks with a higher percentage of PDMS backbone exhibit higher storage modulus but also the gel transition temperature shifts to higher temperatures for the network blends containing a higher concentration of PDMS.

Additionally, for blends based on FS950 and FS3000, the differences between the modulus of PPO and PDMS polymers in the rubbery plateau region are the highest (about 3 orders of magnitude). The modulus and phase angle of blends based on FS950 exhibit a long horizontal line with negligible variations overlapping with the pure DPBM-FS950_r0.7 regardless of the composition and the stoichiometric ratio; it means these glassy blends show small chain mobility before their T_g so that the deformations could not be measured by rheometry analysis (Figure 4i). At elevated temperatures, the viscoelastic behavior of the DA network blends varies based on the morphology of the blends which relies on the composition of the two polymers, the maleimide-to-furan stoichiometric ratio, and the molar mass of the PDMS chain. The effect of morphology becomes more tangible in blends where the phase separation process is faster; for instance, in a constant composition of 50/50, blends containing FS5000 show distinct degelation behaviors (the slop of storage modulus around the degelation point is different) as a function of stoichiometric ratio (Figure 4a) where this distinction in FS3000 and FS950 blends becomes less and less noticeable.

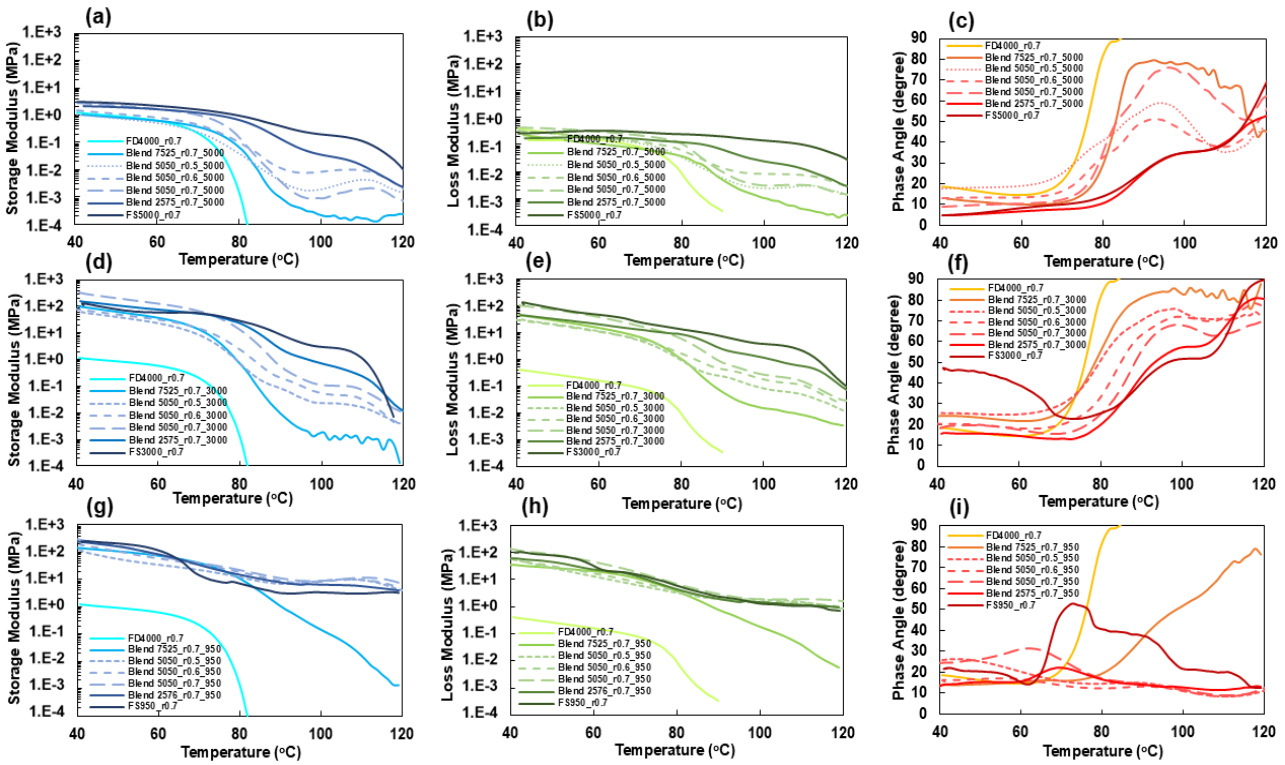

Figure 4. Rheological properties in terms of storage modulus, loss modulus, and phase angle (δ) for pure and blended Diels-Alder networks with different compositions and stoichiometric ratios containing FS5000 (a-c), FS3000 (d-f), or FS950 (g-i). All curves were measured with a temperature ramp of 2 K min^{-1}.

3.5. Barrier properties of Diels-Alder network blends

3.5.1. Barrier properties against water

The transport of molecules, such as water or oxygen, through a polymer occurs in three main stages. Firstly, the permeant molecule is adsorbed onto the surface of the polymer. Secondly, it dissolves (or is absorbed) into the polymer matrix and diffuses through it. Thirdly, the molecule is desorbed from the opposite surface of the polymer[36]. The permeation of water through materials depends on the solubility and diffusivity of water molecules in them, the permeability being the product of the two properties. To evaluate the water solubility in DA networks, the water uptake was analyzed using dynamic vapor sorption analysis (DVS), while water vapor transmission rate (WVTR) tests were made to determine the permeability.

DVS measurements were conducted at 25°C with varying relative humidity (RH%) from 0% to 50% and then 98%. Samples of similar dimensions (6 mm x 6 mm x 0.2 mm) were exposed to each RH% for 360 minutes and finally dried to 0% RH%. Figure 5a compares water vapor sorption results of different pure PPO- and PDMS-based DA networks. After being exposed to each relative humidity, the polymer networks absorb water, rising towards a plateau. The PPO-based DA network DPBM-

FD4000_r0.7 absorbs the highest amount of water (5.6% at 98% RH) due to its less hydrophobic nature. Due to their more hydrophobic nature, the PDMS-based DA networks absorb less water: the pure PDMS-based DA networks DPBM-FS5000_r0.7 and DPBM-FS3000_r0.7 absorb almost the same amount of water (1.4% at 98% RH), while network DPBM-FS950_r0.7 shows a slightly higher water sorption (2.7% at 98% RH). In general, more densely crosslinked networks are associated with a lower amount of water sorption[37], so the higher amount of sorption of the most densely crosslinked DPBM-FS950_r0.7 is likely correlated with its higher mass fraction of bismaleimide and the potential of the maleimide group to form hydrogen bonds. The relationship between polymer structure and water solubility can be explained by theories suggesting that while the free volume within a polymer, which is typically lower for a higher crosslink density, is necessary for water diffusion, it does not directly affect solubility. The presence and concentration of polar groups capable of forming hydrogen bonds with water molecules significantly determine the extent of water absorption, as evidenced by variations in water solubility across different polymer families and by the consistent increase in water uptake with higher concentrations of polar groups within similar polymers[38]. Table 3 evidently shows the positive correlation between the initial concentration of the maleimide and maximum water sorption in either similar pure PPO-based DA networks having different stoichiometric ratios or pure DA networks with the same stoichiometric ratio but different molar masses of PDMS. It shows that the higher the concentration of maleimide groups the higher the water sorption in terms of equilibrium water content.

For the blends, the water sorption decreases with increasing mass ratio of the PDMS backbones (Figures 5b-d), however, this decrease is more obvious for the DA network blends with longer PDMS chains, meaning that water sorption in the blends with FS5000 is more affected by the composition of polymers in the blend. Similarly, changing the maleimide-to-furan stoichiometric ratio in blends with a 50/50 mass ratio of PPO and PDMS results in different concentrations of maleimide groups, with higher maleimide concentrations leading to larger crosslink densities and an increased affinity for water. On top of all, the morphology that evolves by phase separation of immiscible phases can play a role[27]. It is understood that for blends containing shorter PDMS chains, the water sorption is less affected by the composition, the same trend is observed for the effect of stoichiometric ratio (Figures 5c and 5d).

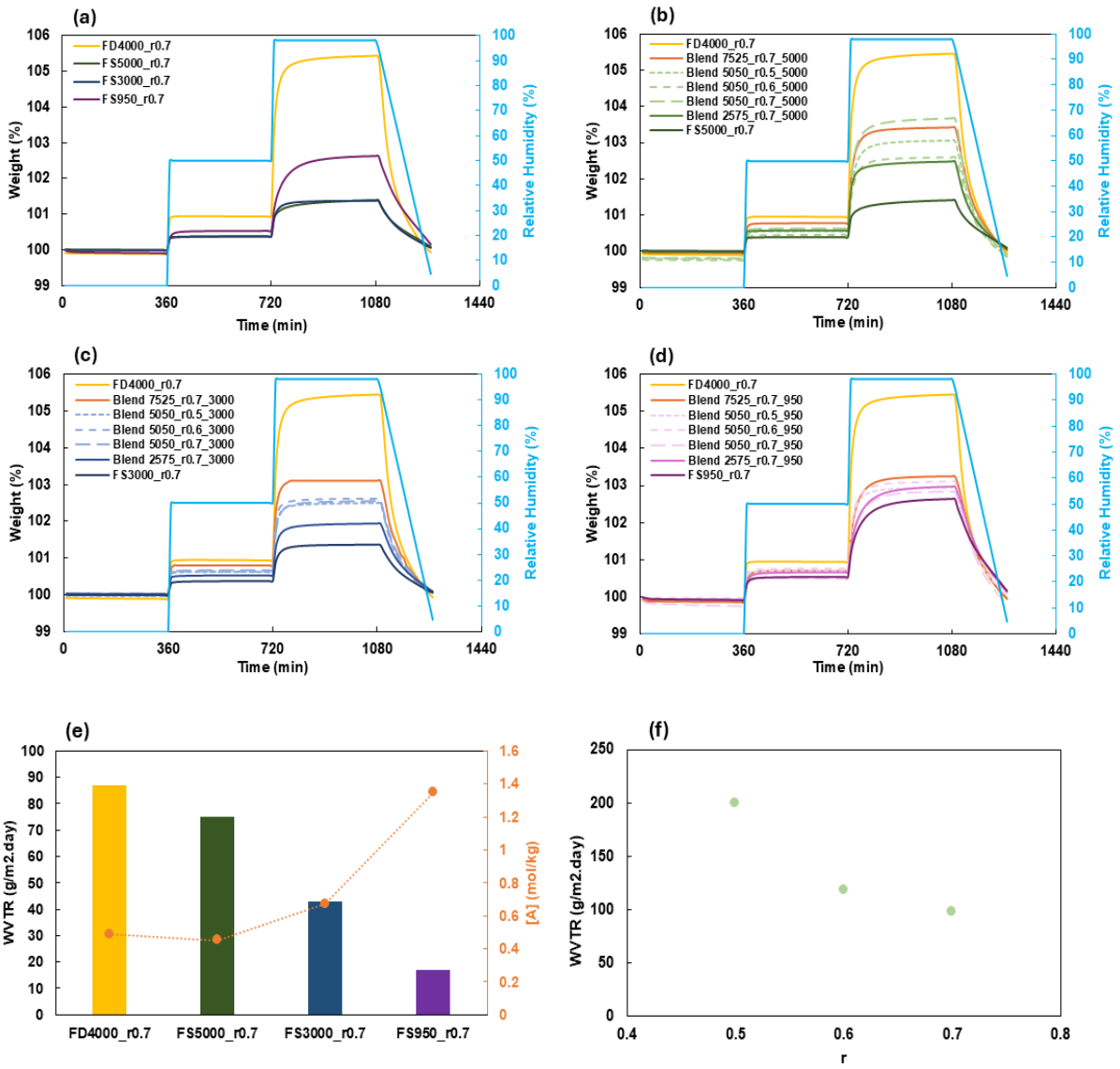

Figure 5. (a) Water sorption curves of pure PPO-based FD4000 and PDMS-based Diels-Alder networks with different molar masses FS5000, FS3000 and, FS950 crosslinked at r=0.7 during 360 min isothermal steps at relative humidities of 0%, 50%, and 98% ending with a ramp of -0.5 % RH min^{-1}. Water sorption curves of pure and blended Diels-Alder networks with different compositions and stoichiometric ratios containing FS5000 (b), FS3000 (c), or FS950 (d) during 360 min isothermal steps at relative humidities of 0%, 50%, and 98% ending with a ramp of -0.5 % RH min^{-1}. (e) Water vapor transmission rate at a relative humidity of 50 %RH at room temperature for pure PPO- and PDMS-based networks crosslinked with a maleimide-to-furan stoichiometric ratio of r=0.7 as well as their room temperature equilibrium Diels-Alder adduct concentration. (f) Water vapor transmission rate of 50/50 blends of FS5000 at a relative humidity of 50 %RH at room temperature as a function of maleimide-to-furan stoichiometric ratio.

Table 3. Maximum water sorption of different networks at relative humidities of 50% and 98% at room temperature (25 °C). The chain molar masses and the initial concentration of the DPBM crosslinker in the network (whether reacted or not) are mentioned for easy comparison.

Network	Maximum sorption at 50% RH (%)	Maximum sorption at 98% RH (%)	Slope of mass increase at RH 98% (% min^{-1})	Chain Molar Mass (g mol^{-1})	$[M]_0$ (mol kg^{-1})
DPBM-FD4000_r0.5	0.6	3.5	0.02	4546	0.34
DPBM-FD4000_r0.6	0.8	3.7	0.07	4546	0.43
DPBM-FD4000_r0.7	1	5.6	0.13	4546	0.49
DPBM-FS5000_r0.7	0.4	1.4	0.03	4961	0.46
DPBM-FS3000_r0.7	0.4	1.4	0.03	3395	0.68
DPBM-FS950_r0.7	0.6	2.7	0.02	907	1.35

Figure 5e demonstrates the water vapor transmission rate of the pure networks and their reversible crosslinking density in terms of the equilibrium concentration of DA adduct ($[A]_{eq}$). In contrast to the water sorption results, the permeation of water decreases by increasing the crosslink density in the PDMS-based DA networks, because of a slower diffusion. As mentioned before, the permeation of water is the product of both solubility and diffusivity, which is why network DPBM-FD4000_r0.7, with a higher density of crosslinks (Table 3), shows higher water permeation compared to DPBM-FS5000_r0.7 due to its more hydrophilic nature.

By looking at Figures 5b and 5f it is possible to compare the water sorption and water permeation, respectively, for 50/50 blends based on FS5000 having different maleimide-to-furan molar ratios. Although the water sorption for blend 5050_r0.7_5000 is the highest, due to the higher concentration of maleimide groups, its water permeation is the lowest due to its higher crosslink density, a lower free volume causing slower diffusion. Here the difference between water sorption and water permeation is clarified. As explained water sorption refers to the uptake of water molecules by the polymer network measured with DVS. Water permeation refers to the passage of water molecules (measured with WVTR) through the polymer network from one side to the other driven by a concentration gradient. In general, water sorption and water permeation in polymer networks are related yet distinct processes. It was discussed that PPO polymer chains in DA blend networks are slightly hydrophilic; they can attract and retain higher amounts of water. The presence in the polymer network of functional groups capable of hydrogen bonding with water molecules such as maleimide groups can enhance water uptake[39]. However, increasing the concentration of these groups by increasing the stoichiometric ratio in networks increases the crosslink density (decreases the free volume) and changes the final behavior concerning water permeation; it means the water permeation will decrease. A high density of the

crosslinks restricts the mobility of polymer chains, which can slow down the diffusion of water molecules through the polymer matrix, leading to a lower water vapor transmission rate (Figure 5f). Generally, in phase-separated blends consisting of two immiscible polymers, where each phase exhibits a different hydrophobicity, the results of water sorption and water permeation tests will differ significantly, not only due to the distinct properties of each polymer network (polarity and crosslink density) but also depending on the morphology of the blend and test orientation[40,41]. In general, the morphology of polymer blends significantly affects the permeation of gases. This is because the structure, size, and distribution of the different phases within the polymer blend can create pathways or barriers that influence the movement of gases through the material, known as the tortuosity effect[36]. Particularly in a bi-layer structure, the water sorption and permeation results depend on the thickness of the layers[42]. In the next sections, the relation between the resistance of each layer against permeation and the overall permeation will be elaborated.

3.5.2. Barrier properties against oxygen

The oxygen transmission rate (OTR) of a film is defined as the steady-state rate at which oxygen gas permeates through a polymer film under specified conditions of film thickness, temperature, relative humidity, and oxygen partial pressure difference over the film. The oxygen transmission rate through films of pure DA networks and their 50/50 blends (r=0.7) is shown in Figure 6a. At a constant stoichiometric ratio of r=0.7, the PDMS-based DA networks DPBM-FS3000_r0.7 and DPBM-FS5000_r0.7 show oxygen transmission rates of 48420±120 cc m^{-2} day^{-1} and 113110±120 cc m^{-2} day^{-1}, respectively, which are about 5 and 12 times higher than the OTR value of the PPO-based network (9426±46 cc m^{-2} day^{-1} for DPBM-FD4000_r0.7). First, the non-polar siloxane backbone increases the solubility of oxygen, and secondly, the molecular structure that contains long chains of silicon and oxygen atoms, with methyl groups attached to the siloxane backbone, which results in a high free volume fraction[43], allows gas molecules to diffuse through the material easily, resulting in the high permeation rate of oxygen through PDMS-based networks[44]. However, in DPBM-FS950_r0.7 both the high crosslink density (reduced free volume) and the polarity and aromaticity of DPBM, present at a higher concentration, are the reasons why DPBM-FS950_r0.7 exhibits more resistance to the permeation of oxygen (6774±2 cc/m^2.day). Blending two polymers with distinct polarities allows a wide adjustment of the barrier properties against oxygen. The measured OTR for network blends composed of PPO/PDMS are detailed in Figures 6b-d, together with theoretical OTR values calculated using rules of mixtures. The upper bound rule of mixtures (UBRM) and lower bound rule of mixtures (LBRM) are expressed in Equations 5.1 and 5.2, respectively:

$$OTR_{blend(UBRM)} = W_{PPO} \times OTR_{PPO} + W_{PDMS} \times OTR_{PDMS}$$ Equation 1

$$OTR_{blend(LBRM)} = \frac{1}{\frac{W_{PPO}}{OTR_{PPO}} + \frac{W_{PDMS}}{OTR_{PDMS}}}$$ Equation 2

Where $OTR_{blend\ (UBRM)}$ and $OTR_{blend\ (LBRM)}$ are the OTR values for the blends, estimated by the upper and lower bound rule of mixtures calculations, respectively, and w_{PPO} and w_{PDMS} are mass fractions of the PPO- and PDMS-based networks in the blends. The upper bound rule of mixtures assumes permeation through phases in parallel, while the lower bound rule of mixtures (LBRM) assumes permeation through phases in series. The measured value for blend 5050_r0.7_5000 is close to the LBRM value, suggesting that the permeation of oxygen through this blend happens predominantly through oxygen resistances in series, which is consistent with the morphology observations. This behavior changes in blends containing FS3000 and FS950, for which the measured OTR values follow the UBRM more closely. This behavior suggests that the morphology of the blends changed predominately. As shown in SEM results (Figures 1b, 1e, and 1h), for a constant stoichiometric ratio, a lower length of the PDMS chains retards the phase separation process, while it increases the concentration of DA functional groups in FS3000 and FS950 and accelerates the crosslinking reaction, preventing the formation of a bi-layer morphology.

Altering the maleimide-to-furan stoichiometric ratio in DA network blends with a 50/50 composition impacts the oxygen transmission rate (Figure 6e): increasing the stochiometric ratio increases the OTR value of blends based on FS5000, while it decreases the OTR value in the blends using FS3000 and FS950. In general, the higher crosslink density and the higher concentration of polar groups resulting from a higher stoichiometric ratio led to a lower free volume in the network, restricting the diffusion of gas molecules, and a lower solubility of oxygen, respectively. The higher permeation rate caused by increasing the stoichiometric ratio in blends containing FS5000 implies that the role of the bi-layer morphology in controlling the oxygen transmission associated with the lack of a uniform layer of hydrophilic PPO empowers the role of the increased crosslink density. It means the concentration of crosslinks increases with the stoichiometric ratio at r=0.7, and the faster kinetics of the DA reaction limits the complete segregation of phases; in this case, the presence of PDMS domains in the PPO phase increases the possibility of oxygen permeation.

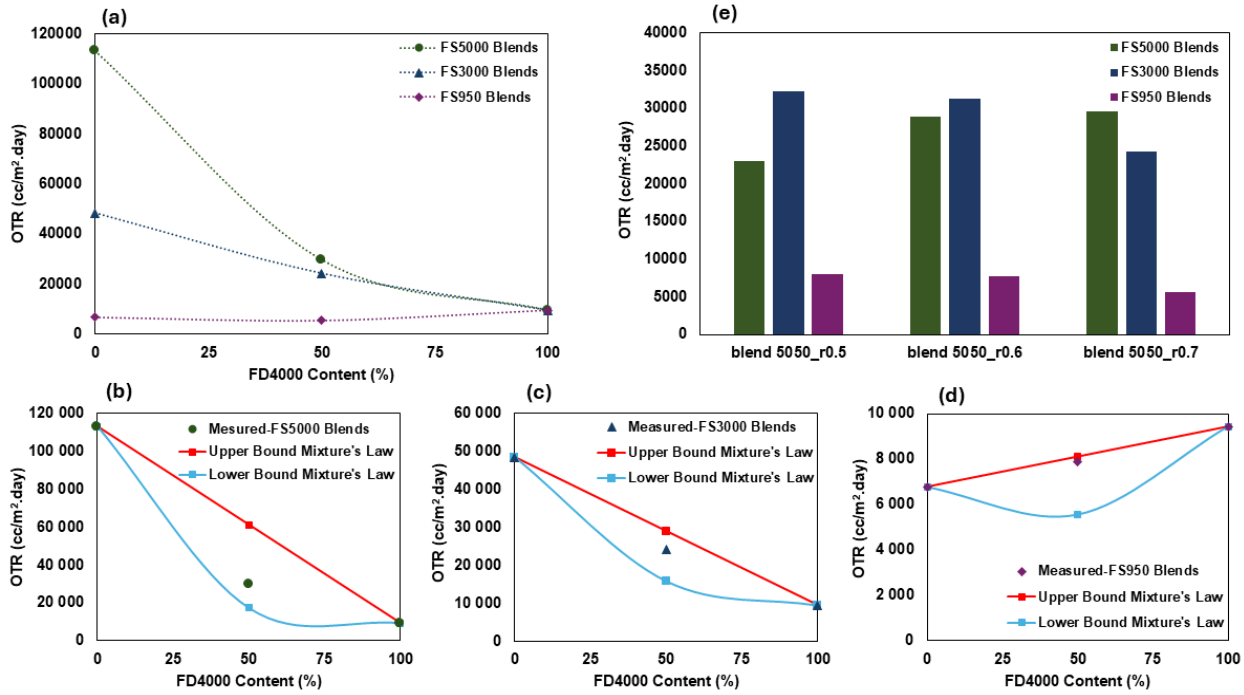

Figure 6. Oxygen transmission rate tests for (a) pure networks and blends of PPO-based FD4000 with PDMS-based FS5000 (green), FS3000 (blue) and FS950 (purple) and simulations of the Upper and Lower Bound Rules of Mixtures for blends with (b) FS5000, (c) FS3000 and (d) FS950, and (e) for 50/50 PPO/PDMS blends as a function of stoichiometric ratio. All values were measured at 50% relative humidity at room temperature.

3.6. Mechanical properties of Diels-Alder network blends

The mechanical properties of the dynamic covalent networks were assessed through stress-strain tests in tensile mode at room temperature. With an elongation at break of up to more than 400% strain, the PPO-based DPBM-FD4000_r0.7 shows the highest elongation among the DA networks. Nevertheless, the PDMS-based DA polymers, having a maximum elongation that is half of the PPO-based DA network or less, exhibit tensile strengths that are 3, 6, or even 30 times larger, for FS5000, FS3000, and FS950-based networks, respectively (see Table 4). The blending of the PPO-based flexible DA network with each of these PDMS-based networks yields adaptive covalent networks that could meet the requirements of a wide range of applications, their properties changing from soft and rubbery (FS5000), over harder elastomers (FS3000), to a more rigid and glassy behavior (FS950). Previous studies support this blending effect in the toughening and stiffening of DA networks[45]. The strain and stress at the break as well as the Young's modulus of the network blends with each grade of PDMS, shown in Figures 7b-d and Table 4 illustrate the range of properties achieved by blending in DA networks. As evident, both composition and stoichiometric ratio have their impact on the mechanical properties. Decreasing the molar mass of the PDMS chains from FS5000 to FS3000 and finally to FS950 at a constant stoichiometric ratio of r=0.7 increases crosslink density (Table 2). The increased

number of crosslinks leads to a higher stress at break, a higher Young's modulus, and a higher toughness, although the strain at break decreases overall.

Hysteresis is a detrimental characteristic of soft and flexible polymers for dynamic applications since it is directly linked to a lack of recovery of mechanical properties upon cycling. For instance, this would be important for polymer encapsulants for liquid metal-based stretchable electronics, where elastic recovery and linearity of the device are challenges to be addressed[27,46]. Increasing the content of the PDMS phase or stoichiometric ratio can elegantly reduce the hysteresis of the polymer networks, at the expense of sacrificing the flexibility of the polymer network, as shown in Figures 7e and 7f, which demonstrate the room temperature hysteresis of pure and blended DA networks for the first cycle of loading-unloading after exposing them to a maximum force of 0.2 MPa. According to Figure 7e, the hysteresis of DPBM-FD4000_r0.7 is predominantly suppressed by the addition of the PDMS phase. In practice, it was proved that a substantial reduction in the energy dissipation behavior of the network is possible by increasing the mass fraction of the PDMS phase or reducing the molar mass of PDMS. Further reduction can be achieved by increasing the maleimide-to-furan molar ratio (Figure 7f). Despite the general rules that were explained blend 5050_r0.7_3000 has more hysteresis in comparison with 5050_r0.7_5000, which is correlated to its morphology. In this morphology (Figure 1e) the PDMS layer of the FS3000 network is not uniformly formed. The disconnection between PDMS-rich phases in this blend is thought to lead to a higher hysteresis in this blend. In general, soft and self-healing polymers especially those networks based on dynamic bonds are prone to high hysteresis due to their dynamics that rely on high chain mobility. Therefore, it is important to design network blends that balance low hysteresis with good self-healing properties.

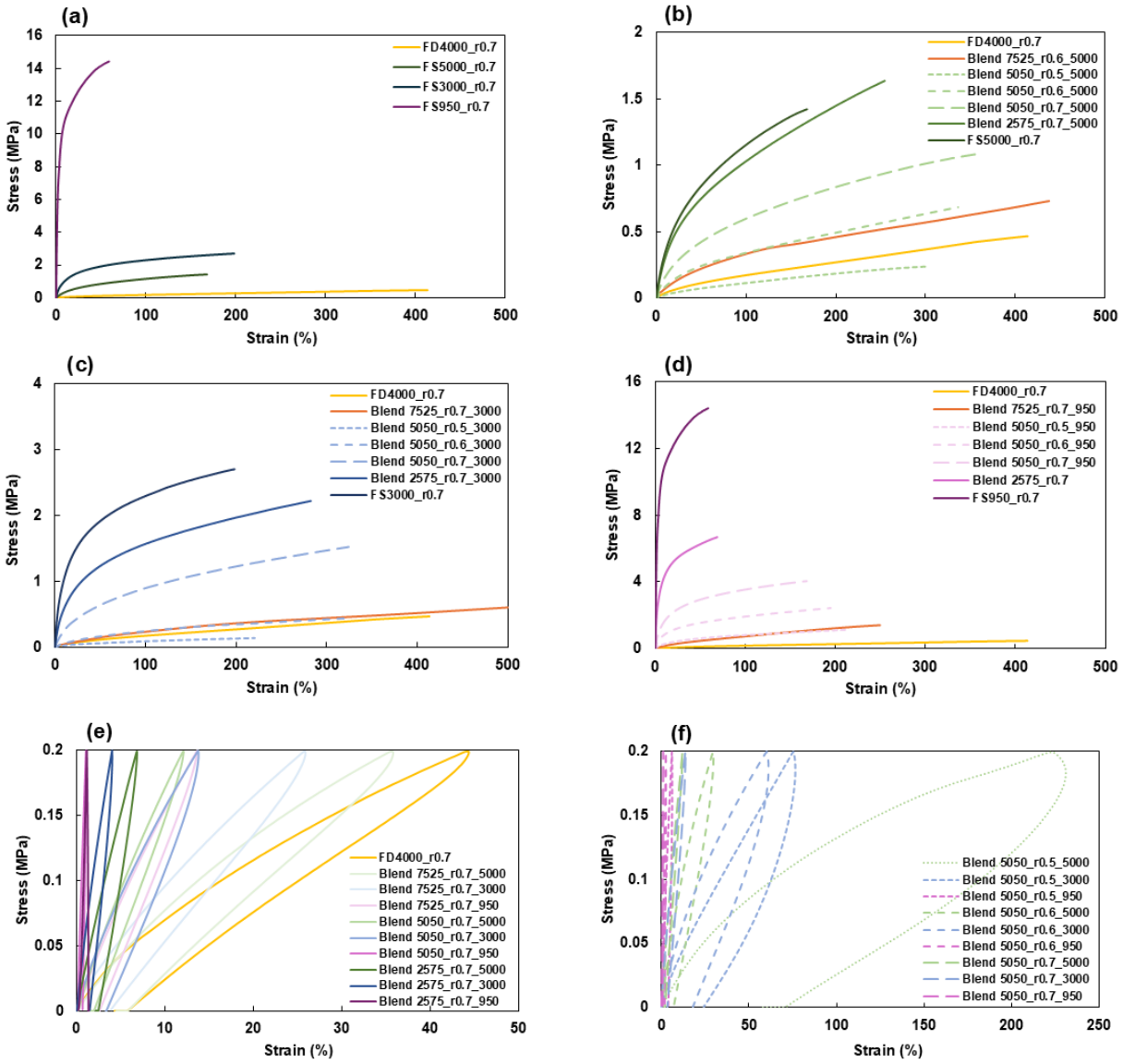

Figure 7. Stress-strain curves of (a) pure PPO-based FD4000 and PDMS-based Diels-Alder networks with different molar masses of FS5000, FS3000 and, FS950 crosslinked at r=0.7 based on the average of five replicants. Mechanical properties in pure and Diels-Alder network blends with different compositions and stoichiometric ratios containing FS5000 (b), FS3000 (c), or FS950 (d). All networks were strained at a rate of 60 % min^{-1} at room temperature. (e) First cycle hysteresis of Diels-Alder network blends after the introduction of different PDMS grades compared to pure DPBM-FD4000_r0.7 as functions of composition. (f) First cycle hysteresis of Diels-Alder network blends with a 50/50 composition having different stoichiometric ratios.

Table 4. The summary of mechanical properties of pure Diels-Alder networks. All data was obtained from stress-strain tests at room temperature (25 °C). Toughness values are calculated from the area under the average stress-strain curves.

Network	Strain at the break (%)	Stress at the break (MPa)	Young's Modulus (MPa)	Toughness (j m^{-3})
DPBM-FD4000_r0.7	413.4±9.7	0.4±0.0	1.2±0.4	112.7
DPBM-FS5000_r0.7	167.9±14.8	1.4±0.1	2.4±0.0	166.2
DPBM-FS3000_r0.7	198.2±31.9	2.7±0.0	26.6±0.9	423.4
DPBM-FS950_r0.7	58.9±0.0	14.4±0.0	470.5±0.0	725.5

3.7. Self-healing properties of Diels-Alder network blends

One of the biggest motivations for using dynamic covalent networks based on DA chemistry is their self-healing behavior[47, 48]. To assess the self-healing efficiency of all pure and blended DA networks, a healing process at room temperature was performed. The bar charts in Figures 8a and 8b demonstrate the mechanical healing efficiencies of different pure and blended networks containing FS5000 and FS3000, respectively, in terms of strain at break, stress at break, and Young's modulus. It is obvious from both graphs that pure DPBM-FD4000_r0.7 shows superb recovery of mechanical properties at room temperature. According to the results, it can be concluded that at a constant stoichiometric ratio of r=0.7, PDMS-based DA polymers FS5000 and FS3000 suffer from a lower healing efficiency. Figure 8b states that in a constant composition and stoichiometric ratio, FS3000 blends have lower healing efficiency than FS5000 blends. This lower efficiency is associated with the higher crosslink density of a dynamic network consisting of shorter PDMS chains. Decreasing the stoichiometric ratio in the blends from 0.7 to 0.5 decreases the crosslink density, hence increasing the chain mobility by providing more free volume, reducing the network stiffness, and increasing the length of the flexible polymer segments between the crosslinks[49]. This results in a polymer network that is more flexible with greater movement of individual polymer chains. This will eventually enhance the dynamic nature of reversible crosslinks leading to a DA network blend with improved self-healing properties. Owing to this adaptability of DA bonds, blend 5050_r0.5_5000 and blend 5050_r0.5_3000 recover 100% and 42% initial strain after the healing process, which are the highest values compared to their counterparts. It should also be mentioned that in constant stoichiometric conditions for DPBM-FD4000 and DPBM-FS5000 despite the comparable concentration of crosslinks the healing efficiency of the PDMS-based network is lower owing to stronger DA bonds that do not tend to be as reversible as bonds in the PPO-based network. The DA bond strength not only relies on the type of diene and dienophile but also the chemical groups connected to them. The adjacent groups play an important role in stability of the DA

bond. In the furan-maleimide DA systems studied in this work, the dynamic DA bonds in a PDMS-based network are stronger than those in a PPO-based network due to differences in polymer chain polarity and steric effects of the contributing groups connected to the furan and maleimide moieties. PDMS is a highly nonpolar polymer, whereas PPO has a higher polarity. In a less polar chain like PDMS, DA bonds experience less interference from competing intermolecular interactions, leading to stronger bond formation. Also, the higher free volume in PDMS minimizes steric hindrance, allowing DA bonds to form in a more stable conformation.

Blends consisting of FS950 could barely heal at room temperature and showed no recovery after the healing process since these glassy and thermoset networks are still vitrified at a healing temperature below their high glass transition temperature. The concentration of reversible crosslinks as not permanent junctions can be estimated by the concentration of DA adducts in equilibrium conditions shown in Table 2. In a constant stoichiometric ratio, for FS950 this concentration is 3 times more than FS5000 and 2 times more than FS3000 (1.34, 0.67, and 0.45 mol g^{-1} for FS950, FS3000, and FS5000, respectively). The high crosslink density of FS950 demolishes the self-healing ability at ambient and slightly elevated temperatures since the healing temperatures are well below its glass transition temperature.

Increasing the thermal energy by elevating the temperature improves the chain mobility and self-healing performance[50]. Hence, the healing process was carried out at 60 ^{o}C to investigate whether there is room for improving the self-healing performance in moderately crosslinked network blends here based on FS3000. The result of this healing process is shown in contrast to the results of the room temperature healing process in terms of the toughness recovery in Figure 8c. In general, for these blends, increasing the healing temperature leads to better recovery of their mechanical properties.

Concerning the objectives of this work, it should be noted that the recovery of mechanical properties is a crucial factor and a key consideration in the selection and design of materials for soft electronics such as polymer encapsulants for liquid metal-based stretchable electronics[51]. These devices frequently experience substantial mechanical stress and exposure to diverse environmental conditions. High recovery of certain properties like elasticity, stretchability, and durability guarantees the functional ability and reliability of the devices throughout their intended lifespan[52]. There is always a trade-off between contradicting properties, so understanding the structure-property relationships and linking these properties to intended application requirements helps to play with the design factors for further optimizations[53,54,55,56].

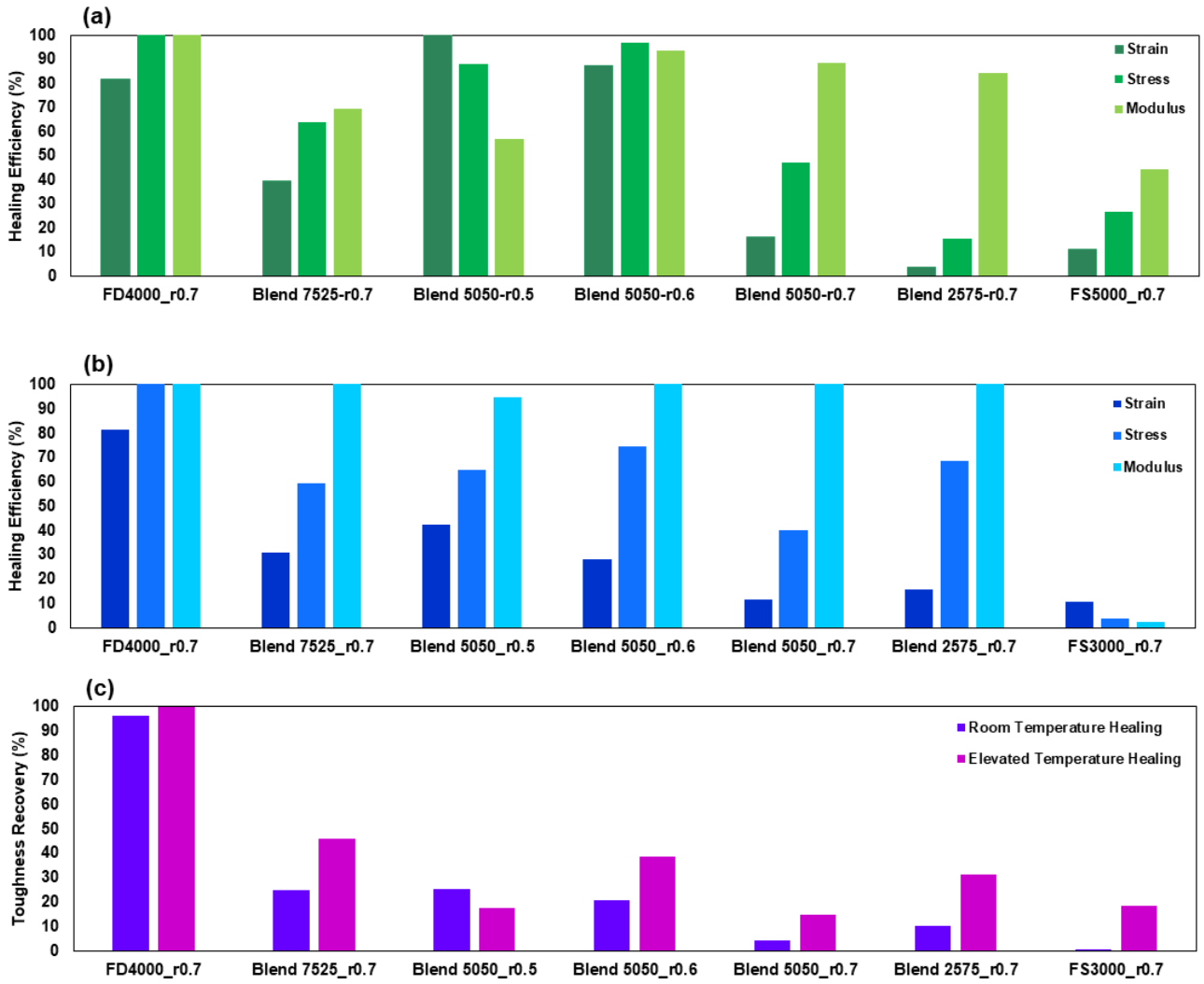

Figure 8. Mechanical healing efficiencies of pure and blended Diels-Alder networks containing FS5000 (a) or FS3000 (b) in terms of strain at break, stress at break, Young's modulus, and toughness after 1-week healing at room temperature. (c) Comparison of recovery of toughness after healing at room temperature and at 60 °C in pure and blended Diels-Alder networks containing FS3000.

4. Conclusions

The study of DA network blends represents a significant advancement in the design of phase-separated blends by leveraging the reversible crosslinks formed via the furan-maleimide DA reaction, combining the hydrophilic polypropylene oxide (PPO) backbone with the hydrophobic polydimethylsiloxanes (PDMS) of varying chain lengths. The research demonstrates how the phase behavior of these network blends is intricately governed by multiple factors. First, the mass ratio of PPO to PDMS changes the morphology from dilute droplet-dispersed morphology to layered structures as the PDMS content increases. Second, decreasing the maleimide-to-furan stoichiometric ratio at a constant 50/50 mass ratio of the two polymers results in higher purity and uniformity of the bi-layer microstructure, mediated by a postponed gelation due to slower DA reaction kinetics. Third, this work focused on the

role of molar mass of the PDMS at mass ratio and stoichiometric ratio. Lowering the PDMS molar mass enhanced the compatibility between the furan-functionalized PPO and PDMS and the stability of the blend thermodynamics, while also increasing the DA reaction kinetics at the higher concentrations of furan and maleimide. Judicious choices of these blend design parameters ultimately leads to the formation of kinetically trapped morphologies with desired combinations of properties. Finally, the solvent extraction time during the wet blending emerges as an additional, critical process parameter affecting the final morphology. Postponing the gelation by halting or slowing down the solvent evaporation provides more time for the network blend to separate into purer phases.

Low PDMS molar masses and short gelation times led to near homogeneous blends, whereas higher PDMS contents, higher PDMS molar masses, lower stoichiometric ratios resulted in separate PDMS and PPO phases, with a PPO interphase with finer PDMS droplets for longer gelation times. The bilayer blends seamlessly combine the advantages properties of the pure networks. The excellent self-healing and barrier against oxygen of the PPO matrix are combined with the barrier against water and the higher stiffness of the PDMS matrix (best blends with best combinations of properties).

focusing on the mechanical and self-healing properties of the blends reveals contrasting outcomes based on PDMS chain length: longer chains accelerate the phase separation process, slow down reaction kinetics, and finally yield elastomeric networks with autonomous self-healing properties, whereas shorter PDMS chains restrict phase separation, accelerate reaction kinetics, and result in thermoset networks with limited self-healing properties under ambient conditions. Overall, the strategic manipulation of these factors enables the tailored design of DA network blends with diverse properties suitable for various applications. However, achieving an optimal balance among barrier properties, mechanical properties, and self-healing properties remains pivotal in the development of advanced polymer encapsulants. This interdisciplinary approach underscores the importance of structure-property-application relationships in advancing materials science and engineering.

5. References

(1) Robeson, L. M. Fundamentals of Polymer Blends. *Polymer Blends* **2007**, 11–64. https://doi.org/10.3139/9783446436503.002.

(2) Idumah, C. I. Recent Advancements in Self-Healing Polymers, Polymer Blends, and Nanocomposites. *Polymers and Polymer Composites* **2021**, *29* (4), 246–258. https://doi.org/10.1177/0967391120910882.

(3) Li, H.; Sundararaj, U. Morphology Development of Polymer Blends in Extruder: The Effects of Compatibilization and Rotation Rate. *Macromol Chem Phys* **2009**, *210* (10), 852–863. https://doi.org/10.1002/macp.200800543.

(4) Paul, D. R.; Barlow, J. W. Polymer Blends (or Alloys). *Journal of Macromolecular Science, Part C* **1980**, *18* (1), 109–168. https://doi.org/10.1080/00222358008080917.

(5) Li, L.; Miesch, C.; Sudeep, P. K.; Balazs, A. C.; Emrick, T.; Russell, T. P.; Hayward, R. C. Kinetically Trapped Co-Continuous Polymer Morphologies through Intraphase Gelation of Nanoparticles. *Nano Lett* **2011**, *11* (5), 1997–2003. https://doi.org/10.1021/nl200366z.

(6) Li, D.; Huo, M.; Liu, L.; Zeng, M.; Chen, X.; Wang, X.; Yuan, J. Overcoming Kinetic Trapping for Morphology Evolution during Polymerization-Induced Self-Assembly. *Macromol Rapid Commun* **2019**, *40* (16), 1–5. https://doi.org/10.1002/marc.201900202.

(7) Du, J.; Li, Y.; Wang, J.; Wang, C.; Liu, D.; Wang, G.; Liu, S. Mechanically Robust, Self-Healing, Polymer Blends and Polymer/Small Molecule Blend Materials with High Antibacterial Activity. *ACS Appl Mater Interfaces* **2020**, *12* (24), 26966–26972. https://doi.org/10.1021/acsami.0c06591.

(8) Safaei, A.; Terryn, S.; Vanderborght, B.; Van Assche, G.; Brancart, J. Toughening and Stiffening in Thermoreversible Diels-Alder Polymer Network Blends. *Macromolecules* **2022**, *56* (11), 4325–4335. https://doi.org/10.1021/acs.macromol.2c02558.

(9) Li, L.; Peng, X.; Zhu, D.; Zhang, J.; Xiao, P. Recent Progress in Polymers with Dynamic Covalent Bonds. *Macromol Chem Phys* **2023**, *224* (20), 1–25. https://doi.org/10.1002/macp.202300224.

(10) Dahlke, J.; Zechel, S.; Hager, M. D.; Schubert, U. S. How to Design a Self-Healing Polymer: General Concepts of Dynamic Covalent Bonds and Their Application for Intrinsic Healable Materials. *Adv Mater Interfaces* **2018**, *5* (17), 1–14. https://doi.org/10.1002/admi.201800051.

(11) Chen, T.; Fang, L.; Li, X.; Gao, D.; Lu, C.; Xu, Z. Self-Healing Polymer Coatings of Polyurea-Urethane/Epoxy Blends with Reversible and Dynamic Bonds. *Prog Org Coat* **2020**, *147* (June), 105876. https://doi.org/10.1016/j.porgcoat.2020.105876.

(12) Chen, T.; Fang, L.; Li, X.; Gao, D.; Lu, C.; Xu, Z. Self-Healing Polymer Coatings of Polyurea-Urethane/Epoxy Blends with Reversible and Dynamic Bonds. *Prog Org Coat* **2020**, *147* (June), 105876. https://doi.org/10.1016/j.porgcoat.2020.105876.

(13) Orozco, F.; Li, J.; Ezekiel, U.; Niyazov, Z.; Floyd, L.; Lima, G. M. R.; Winkelman, J. G. M.; Moreno-Villoslada, I.; Picchioni, F.; Bose, R. K. Diels-Alder-Based Thermo-Reversibly Crosslinked Polymers: Interplay of Crosslinking Density, Network Mobility, Kinetics and Stereoisomerism. *Eur Polym J* **2020**, *135* (May), 109882. https://doi.org/10.1016/j.eurpolymj.2020.109882.

(14) Liu, Y. L.; Chuo, T. W. Self-Healing Polymers Based on Thermally Reversible Diels-Alder Chemistry. *Polym Chem* **2013**, *4* (7), 2194–2205. https://doi.org/10.1039/c2py20957h.

(15) Safaei, A.; Terryn, S.; Vanderborght, B.; Van Assche, G.; Brancart, J. The Influence of the Furan and Maleimide Stoichiometry on the Thermoreversible Diels–Alder Network Polymerization. *Polymers (Basel)* **2021**, *13* (15). https://doi.org/10.3390/polym13152522.

(16) Terryn, S.; Brancart, J.; Roels, E.; Verhelle, R.; Safaei, A.; Cuvellier, A.; Vanderborght, B.; Van Assche, G. Structure-Property Relationships of Self-Healing Polymer Networks Based on Reversible Diels-Alder Chemistry. *Macromolecules* **2022**, *55* (13), 5497–5513. https://doi.org/10.1021/acs.macromol.2c00434.

(17) Chen, L.; Pan, D.; He, H. Morphology Development of Polymer Blend Fibers along Spinning Line. *Fibers* **2019**, *7* (4). https://doi.org/10.3390/fib7040035.

(18) Mou, L.; Qi, J.; Tang, L.; Dong, R.; Xia, Y.; Gao, Y.; Jiang, X. Highly Stretchable and Biocompatible Liquid Metal-Elastomer Conductors for Self-Healing Electronics. *Small* **2020**, *16* (51), 1–9. https://doi.org/10.1002/smll.202005336.

(19) Sahraeeazartamar, F.; Terryn, S.; Sangma, R. N.; Krack, M.; Peeters, R.; Van den Brande, N.; Deferme, W.; Vanderborght, B.; Van Assche, G.; Brancart, J. Diels–Alder Network Blends as Self-Healing Encapsulants for Liquid Metal-Based Stretchable Electronics. *ACS Applied Materials and Interfaces* **2024**. https://doi.org/10.1021/acsami.4c07129.

(20) Strachota, B.; Morand, A.; Dybal, J.; Matějka, L. Control of Gelation and Properties of Reversible Diels-Alder Networks: Design of a Self-Healing Network. *Polymers (Basel)* **2019**, *11* (6), 1–23. https://doi.org/10.3390/polym11060930.

(21) Fortunato, G.; van den Tempel, P.; Bose, R. K. Advances in Self-Healing Coatings Based on Diels-Alder Chemistry. *Polymer (Guildf)* **2024**, *294* (January), 126693. https://doi.org/10.1016/j.polymer.2024.126693.

(22) Toncelli, C.; De Reus, D. C.; Picchioni, F.; Broekhuis, A. A. Properties of Reversible Diels-Alder Furan/Maleimide Polymer Networks as Function of Crosslink Density. *Macromol Chem Phys* **2012**, *213* (2), 157–165. https://doi.org/10.1002/macp.201100405.

(23) Safaei, A.; Terryn, S.; Vanderborght, B.; Van Assche, G.; Brancart, J. The Influence of the Furan and Maleimide Stoichiometry on the Thermoreversible Diels–Alder Network Polymerization. *Polymers (Basel)* **2021**, *13* (15). https://doi.org/10.3390/polym13152522.

(24) Safaei, A.; Brancart, J.; Wang, Z.; Yazdani, S.; Vanderborght, B.; Van Assche, G.; Terryn, S. Fast Self-Healing at Room Temperature in Diels–Alder Elastomers. *Polymers (Basel)* **2023**, *15* (17). https://doi.org/10.3390/polym15173527.

(25) Appuhamillage, G. A.; Reagan, J. C.; Khorsandi, S.; Davidson, J. R.; Voit, W.; Smaldone, R. A. 3D Printed Remendable Polylactic Acid Blends with Uniform Mechanical Strength Enabled by a Dynamic Diels-Alder Reaction. *Polym Chem* **2017**, *8* (13), 2087–2092. https://doi.org/10.1039/c7py00310b.

(26) Chen, T.; Fang, L.; Li, X.; Gao, D.; Lu, C.; Xu, Z. Self-Healing Polymer Coatings of Polyurea-Urethane/Epoxy Blends with Reversible and Dynamic Bonds. *Prog Org Coat* **2020**, *147* (June), 105876. https://doi.org/10.1016/j.porgcoat.2020.105876.

(27) Sahraeeazartamar, F.; Terryn, S.; Sangma, R. N.; Krack, M.; Peeters, R.; Van den Brande, N.; Deferme, W.; Vanderborght, B.; Van Assche, G.; Brancart, J. Diels–Alder Network Blends as Self-Healing Encapsulants for Liquid Metal-Based Stretchable Electronics. *ACS Applied Materials and Interfaces* **2024**. https://doi.org/10.1021/acsami.4c07129.

(28) Paul, D. R.; Barlow, J. W. Polymer Blends (or Alloys). *Journal of Macromolecular Science, Part C* **1980**, *18* (1), 109–168. https://doi.org/10.1080/00222358008080917.

(29) Li, D.; Huo, M.; Liu, L.; Zeng, M.; Chen, X.; Wang, X.; Yuan, J. Overcoming Kinetic Trapping for Morphology Evolution during Polymerization-Induced Self-Assembly. *Macromol Rapid Commun* **2019**, *40* (16), 1–5. https://doi.org/10.1002/marc.201900202.

(30) Li, L.; Miesch, C.; Sudeep, P. K.; Balazs, A. C.; Emrick, T.; Russell, T. P.; Hayward, R. C. Kinetically Trapped Co-Continuous Polymer Morphologies through Intraphase Gelation of Nanoparticles. *Nano Lett* **2011**, *11* (5), 1997–2003. https://doi.org/10.1021/nl200366z.

(31) Bond Energy and Enthalpy. *Chegg*.

(32) Remiro, P. M.; Cortazar, M.; Calahorra, E.; Calafel, M. M. The Effect of Crosslinking and Miscibility on the Thermal Degradation of an Uncured and an Amine-Cured Epoxy Resin Blended with Poly(ε-Caprolactone). *Polym Degrad Stab* **2002**, *78* (1), 83–93. https://doi.org/10.1016/S0141-3910(02)00122-2.

(33) Han, S. O.; Lee, D. W.; Han, O. H. Thermal Degradation of Crosslinked High Density Polyethylene. *Polym Degrad Stab* **1999**, *63* (2), 237–243. https://doi.org/10.1016/S0141-3910(98)00098-6.

(34) Zhang, Z.; Li, Q.; Yesildag, C.; Bartsch, C.; Zhang, X.; Liu, W.; Loebus, A.; Su, Z.; Lensen, M. C. Influence of Network Structure on the Crystallization Behavior in Chemically Crosslinked Hydrogels. *Polymers (Basel)* **2018**, *10* (9). https://doi.org/10.3390/polym10090970.

(35) Mangialetto, J.; Verhelle, R.; Van Assche, G.; Van Den Brande, N.; Van Mele, B. Time-Temperature-Transformation, Temperature-Conversion-Transformation, and Continuous-Heating-Transformation Diagrams of Reversible Covalent Polymer Networks. *Macromolecules* **2021**, *54* (1), 412–425. https://doi.org/10.1021/acs.macromol.0c02491.

(36) Prasad, K.; Nikzad, M.; Sbarski, I. Permeability Control in Polymeric Systems: A Review. *Journal of Polymer Research* **2018**, *25* (11). https://doi.org/10.1007/s10965-018-1636-x.

(37) Chandy, M. C.; Pillai, V. N. R. Water Sorption and Water Binding Properties of Crosslinked Polyacrylamides: Effect of Macromolecular Structure and Crosslinking. *Polym Int* **1995**, *37* (1), 39–45. https://doi.org/10.1002/pi.1995.210370105.

(38) Gilormini, P.; Verdu, J. On the Role of Hydrogen Bonding on Water Absorption in Polymers. *Polymer (Guildf)* **2018**, *142*, 164–169. https://doi.org/10.1016/j.polymer.2018.03.033.

(39) Bouvet, G.; Dang, N.; Cohendoz, S.; Feaugas, X.; Mallarino, S.; Touzain, S. Impact of Polar Groups Concentration and Free Volume on Water Sorption in Model Epoxy Free Films and Coatings. *Prog Org Coat* **2016**, *96*, 32–41. https://doi.org/10.1016/j.porgcoat.2015.12.011.

(40) John, B.; Thomas, S. P.; Varughese, K. T.; Oommen, Z.; Thomas, S. The Effects of Blend Ratio, Compatibilization and Dynamic Vulcanization on Permeation of Gases through HDPE/EVA Blends. *Journal of Polymer Research* **2011**, *18* (5), 1101–1109. https://doi.org/10.1007/s10965-010-9512-3.

(41) Yue, S.; Zhang, T.; Wang, S.; Han, D.; Huang, S.; Xiao, M.; Meng, Y. Recent Progress of Biodegradable Polymer Package Materials: Nanotechnology Improving Both Oxygen and Water Vapor Barrier Performance. *Nanomaterials* **2024**, *14* (4). https://doi.org/10.3390/nano14040338.

(42) Zabihzadeh Khajavi, M.; Ebrahimi, A.; Yousefi, M.; Ahmadi, S.; Farhoodi, M.; Mirza Alizadeh, A.; Taslikh, M. Strategies for Producing Improved Oxygen Barrier Materials Appropriate for the Food Packaging Sector. *Food Engineering Reviews* **2020**, *12* (3), 346–363. https://doi.org/10.1007/s12393-020-09235-y.

(43) White, R. P.; Lipson, J. E. G. Polymer Free Volume and Its Connection to the Glass Transition. *Macromolecules* **2016**, *49* (11), 3987–4007. https://doi.org/10.1021/acs.macromol.6b00215.

(44) Wu, S.; Zhang, X.; Sun, Y.; Yang, H.; Lin, B.; Han, X.; Chen, P. Study on the Influence of Crosslinking Density and Free Polysiloxan Chain Length on Oxygen Permeability and Hydrophilicity of Multicomponent Silicone Hydrogels. *Colloid Polym Sci* **2021**, 1327–1335. https://doi.org/10.1007/s00396-021-04850-5.

(45) Safaei, A.; Terryn, S.; Vanderborght, B.; Van Assche, G.; Brancart, J. Toughening and Stiffening in Thermoreversible Diels-Alder Polymer Network Blends. *Macromolecules* **2022**, *56* (11), 4325–4335. https://doi.org/10.1021/acs.macromol.2c02558.

(46) Xia, Q.; Wang, S.; Zhai, W.; Shao, C.; Xu, L.; Yan, D.; Yang, N.; Dai, K.; Liu, C.; Shen, C. Highly Linear and Low Hysteresis Porous Strain Sensor for Wearable Electronic Skins. *Composites Communications* **2021**, *26* (March), 100809. https://doi.org/10.1016/j.coco.2021.100809.

(47) Ratwani, C. R.; Kamali, A. R.; Abdelkader, A. M. Self-Healing by Diels-Alder Cycloaddition in Advanced Functional Polymers: A Review. *Prog Mater Sci* **2023**, *131* (April 2022), 101001. https://doi.org/10.1016/j.pmatsci.2022.101001.

(48) Terryn, S.; Brancart, J.; Lefeber, D.; Van Assche, G.; Vanderborght, B. Self-Healing Soft Pneumatic Robots. *Sci Robot* **2017**, *2* (9), 1–13. https://doi.org/10.1126/scirobotics.aan4268.

(49) Yu, K.; Xin, A.; Feng, Z.; Lee, K. H.; Wang, Q. Mechanics of Self-Healing Thermoplastic Elastomers. *J Mech Phys Solids* **2020**, *137*. https://doi.org/10.1016/j.jmps.2019.103831.

(50) Kong, D.; Li, J.; Guo, A.; Zhang, X.; Xiao, X. Self-Healing High Temperature Shape Memory Polymer. *Eur Polym J* **2019**, *120* (July), 109279. https://doi.org/10.1016/j.eurpolymj.2019.109279.

(51) Wang, X.; Zhao, M.; Zhang, L.; Li, K.; Wang, D.; Zhang, L.; Zhang, A.; Xu, Y. Liquid Metal Bionic Instant Self-Healing Flexible Electronics with Full Recyclability and High Reliability. *Chemical Engineering Journal* **2022**, *431* (November 2021). https://doi.org/10.1016/j.cej.2021.133965.

(52) Terryn, S.; Langenbach, J.; Roels, E.; Brancart, J.; Bakkali-Hassani, C.; Poutrel, Q. A.; Georgopoulou, A.; George Thuruthel, T.; Safaei, A.; Ferrentino, P.; Sebastian, T.; Norvez, S.; Iida, F.; Bosman, A. W.; Tournilhac, F.; Clemens, F.; Van Assche, G.; Vanderborght, B. A Review on Self-Healing Polymers for Soft Robotics. *Materials Today*. Elsevier B.V. July 1, 2021, pp 187–205. https://doi.org/10.1016/j.mattod.2021.01.009.

(53) Terryn, S.; Brancart, J.; Roels, E.; Verhelle, R.; Safaei, A.; Cuvellier, A.; Vanderborght, B.; Van Assche, G. Structure-Property Relationships of Self-Healing Polymer Networks Based on Reversible Diels-Alder Chemistry. *Macromolecules* **2022**, *55* (13), 5497–5513. https://doi.org/10.1021/acs.macromol.2c00434.

(54) Sahraeeazartamar, F.; Terryn, S.; Roels, E.; Safaei, A.; drazan jozic; Vanderborght, B.; Assche, G. Van; Brancart, J. Effect of Secondary Particles on Self-Healing and Electromechanical Properties of Polymer Composites Based on Carbon Black and a Diels − Alder Network. *Applied Polymer Materials* **2023**, *5* (10), 7813–7830. https://doi.org/10.1021/acsapm.3c01043.

(55) Sahraeeazartamar, F.; Yang, Z.; Terryn, S.; Jozić, D.; Vanderborght, B.; Van Assche, G.; Brancart, J. Designing Flexible and Self-Healing Electronics Using Hybrid Carbon Black/Nanoclay Composites Based on Diels-Alder Dynamic Covalent Networks. *Macromolecules* **2024**, *57* (2), 539–553. https://doi.org/10.1021/acs.macromol.3c01904.

(56) Jo, Y. Y.; Lee, A. S.; Baek, K. Y.; Lee, H.; Hwang, S. S. Thermally Reversible Self-Healing Polysilsesquioxane Structure-Property Relationships Based on Diels-Alder Chemistry. *Polymer (Guildf)* **2017**, *108*, 58–65. https://doi.org/10.1016/j.polymer.2016.11.040.

FUNDING SOURCES

This work was supported by the FWO-SBO project SUBLIME (S007423N) and the Fonds voor Wetenschappelijk Onderzoek (FWO) Flanders through the junior postdoctoral fellowship of Joost Brancart (12W4719N).

ACKNOWLEDGMENTS

The authors would like to acknowledge Mr. Dimitri Adons and Mrs. Riet Henno for their technical support in oxygen permeability tests. The authors also would like to thank Huntsman Corporation for supplying the Jeffamine D series amine hardeners. This work was supported by the FWO-SBO project SUBLIME (S007423N) and the Fonds voor Wetenschappelijk Onderzoek (FWO) Flanders through the junior postdoctoral fellowship of Joost Brancart (12W4719N).

AUTHOR INFORMATION

Corresponding Author

Joost Brancart − Sustainable Materials Engineering (SUME), Lab Physical Chemistry and Polymer Science (FYSC), B-1050 Brussels, Belgium; Joost Brancart (0000-0002-1735-1515) (orcid.org); Email: joost.brancart@vub.be

Authors

Fatemeh Sahraeeazartamar − Sustainable Materials Engineering (SUME), Lab Physical Chemistry and Polymer Science (FYSC), Vrije Universiteit Brussel (VUB), B-1050 Brussels, Belgium; Fatemeh Sahraeeazartmar (0000-0002-4207-2198) (orcid.org); Email: fatemeh.sahraeeazartamar@vub.be

Nirmayi Sadanand Joshi− Sustainable Materials Engineering (SUME), Lab Physical Chemistry and Polymer Science (FYSC), Vrije Universiteit Brussel (VUB), B-1050 Brussels; Nirmayi Sadanand Joshi (0009-0006-9722-1580) (orcid.org); Email: joshinirmayi@gmail.com

Roos Peeters − Materials and Packaging Research & Services (MPR&S), Institute for Materials Research (IMO-IMOMEC), Hasselt University, Wetenschapspark 27, 3590 Diepenbeek, Belgium; Roos Peeters (0000-0001-7515-802X) (orcid.org); Email: roos.peeters@uhasselt.be

Bram Vanderborght − Brubotics, Vrije Universiteit Brussel (VUB) and IMEC, B-1050 Brussels, Belgium; Bram Vanderborght (0000-0003-4881-9341) (orcid.org); Email: bram.vanderborght@vub.be

Guy Van Assche − Sustainable Materials Engineering (SUME), Lab Physical Chemistry and Polymer Science (FYSC), Vrije Universiteit Brussel (VUB), B-1050 Brussels, Belgium; Guy Van Assche (0000-0003-0452-6272) (orcid.org); Email: guy.van.assche@vub.be

Joost Brancart − Sustainable Materials Engineering (SUME), Lab Physical Chemistry and Polymer Science (FYSC), B-1050 Brussels, Belgium; Joost Brancart (0000-0002-1735-1515) (orcid.org); Email: joost.brancart@vub.be

Author Contributions

Conceptualization, investigation, validation, and writing-original draft (F.S.); Conceptualization, investigation, validation (N.S.J.); oxygen permeability test (R.P.); funding acquisition (B.V.); supervision, writing-review and editing, and funding acquisition (G.V-A.); conceptualization, supervision, writing-review and editing, and funding acquisition (J.B.).